

Theory of electronic magnetoelectric coupling in d^5 Mott insulators

Adrien Bolens*

Department of Physics, University of Tokyo, Hongo, Bunkyo-ku, Tokyo 113-0033, Japan

(Dated: October 3, 2018)

Motivated by recent terahertz (THz) spectroscopy measurements in α - RuCl_3 , we develop a theory for magnetoelectric (ME) effects in Mott insulators of d^5 transition metal ions in an octahedral crystal field. For $4d$ and $5d$ compounds, the relatively wide-spread orbitals favor charge fluctuations of localized electrons to neighboring ions and a significant ME effect from electronic mechanisms is expected. From a three-orbital Hubbard model with strong spin-orbit coupling, we derive the mechanisms for the electric polarization originating from virtual hopping of the localized holes carrying the spins. We consider the electric polarization generated by pairs of spin operators on nearest neighbor bonds with either an edge-sharing geometry (i.e., two ligands are shared) or a corner-sharing geometry (i.e., one ligand is shared). The allowed couplings are first derived using a symmetry approach. Then, we explicitly calculate the coupling constants and evaluate the effective polarization operator in the ground state manifold using perturbation theory and exact diagonalization. The results are relevant when considering the THz optical conductivity of magnetic systems such as some perovskite iridates or Kitaev materials. In particular, they help explain the recent THz optical measurements of α - RuCl_3 for which the electric-dipole-induced contribution has been shown to be strong.

I. INTRODUCTION

Multiferroics are defined by the existence of the static magnetoelectric (ME) effect, i.e., the control of electric polarization by a magnetic field and of magnetization by an electric field¹⁻⁷. In the dynamical regime, the magnetically induced ferroelectricity leads to the emergence of electromagnons, low-lying modes associated with the hybridization of spin waves with the electric polarization⁸⁻¹⁴.

However, ME effects are not limited to multiferroics. In magnetic Mott insulators with lattice inversion invariance and no electric polarization in the ground state, i.e., without the static ME effect and reduction of the symmetry accompanying the long-range ordering, dynamical ME effects are still possible.

Three types of mechanisms for the ME coupling between the local electric polarization \mathbf{P}_{ij} and spin operators at sites i and j are typically considered for multiferroics: (i) the exchange-striction mechanism arising from the symmetric spin exchange interaction $\mathbf{S}_i \cdot \mathbf{S}_j$ ¹⁵, (ii) the spin-current model arising from the antisymmetric spin exchange interaction $\mathbf{S}_i \times \mathbf{S}_j$ (or inverse Dzyaloshinskii-Moriya interaction)¹⁶⁻¹⁸, and (iii) the spin dependent p - d hybridization mechanism, which causes single spin anisotropy¹⁹⁻²¹. Only the mechanism (ii) is allowed in a system with inversion symmetry, whereas the lack of inversion symmetry centered at the middle of bonds and spin sites is necessary for mechanisms (i) and (iii), respectively.

The ME coupling affects the charge dynamics of the electrons in the magnetic energy scale, far below the optical gap of Mott insulators. Thanks to the coupling, the magnetic excitations respond to an AC electric field and can be probed, for example, by measuring the terahertz (THz) dielectric response. This is especially interesting for quantum spin liquids (QSL) with fractionalized excitations, which result in a continuous subgap optical con-

ductivity. This effect has been predicted and observed in some QSLs²²⁻²⁵, and explained with a different kind of ME mechanism. For the single-band Hubbard model, charge effects are possible through virtual hopping of the electrons, which scales as $(t/U)^n$ for loops of size n (with t the hopping amplitude and U the on-site repulsion)²⁶. Even without spin-orbit coupling (SOC), a nontrivial ME coupling arises for odd n , starting from triangular loops, and explains the subgap optical conductivity of gapless QSLs on triangular and kagome lattices^{22,23,27,28}.

More recently, a subgap optical conductivity was observed in the Kitaev material α - RuCl_3 in a series of THz spectroscopy measurements²⁹⁻³³. In a previous work, we showed that the virtual hopping mechanism can be relevant for $n = 2$ (single bonds) when considering multi-orbital systems such as Kitaev materials with strong SOC³⁴.

In this paper, motivated by the THz spectroscopy results in α - RuCl_3 , we derive the general mechanisms for the polarization operators of $4d^5$ and $5d^5$ Mott insulators arising from the electronic charge in t_{2g} orbitals.

More specifically, we consider systems with inversion symmetry and without degeneracy of the local ground states (other than the Kramers degeneracy), so that the low-energy manifold is described with pseudospin-1/2 variables on each site. We focus on systems with d^5 transition metal (TM) ions, each surrounded by an octahedral complex of ligands that connect neighboring TM sites. For $4d$ and $5d$ compounds, the wide-spread orbitals favor charge fluctuations of the localized holes to neighboring ions, so that we expect significant ME effects from purely electronic mechanisms.

Two geometries are considered, the edge-sharing geometry (i.e., two ligands are shared) and the corner-sharing geometry (i.e., one ligand is shared) as shown in Fig. 1.

Our goal is to calculate the effective polarization in the magnetic ground state manifold, i.e., in terms of spin-1/2 operators. Due to time-reversal symmetry, there are no

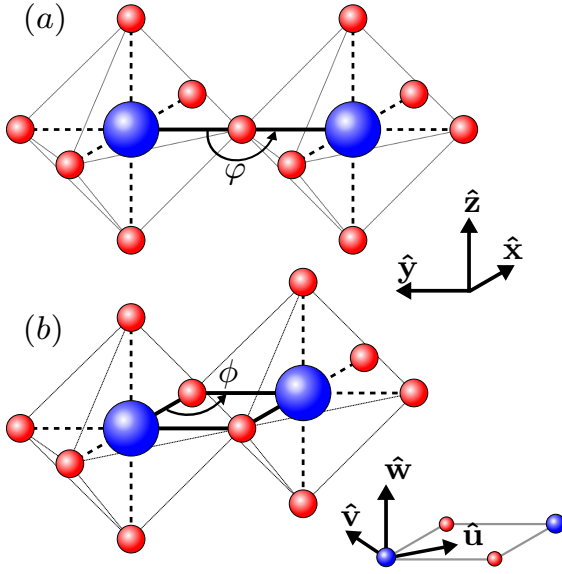


FIG. 1. (a) Corner-sharing and (b) edge-sharing geometries. The blue spheres represent the TM ions and the smaller red spheres the ligands. Deviations from $\phi = 90^\circ$ and $\varphi = 180^\circ$ are considered in Appendices A and B.

one-spin terms and we only consider terms written with two-spin operators from nearest neighbors.

The spin-current model, which lead to the Katsura-Nagaosa-Balatsky (KNB) formula $\mathbf{P}_{ij} \propto \hat{\mathbf{e}}_{ij} \times (\mathbf{S}_i \times \mathbf{S}_j)$ ¹⁶, where $\hat{\mathbf{e}}_{ij}$ is the unit vector parallel to the bond, was originally based on a purely electronic mechanism made possible by finite matrix elements such as $\langle d_{xy} | y | p_x \rangle$ between neighboring TM ions and ligands¹⁶. The same matrix elements have been shown to give rise to additional symmetry-allowed couplings between \mathbf{P}_{ij} and $\mathbf{S}_i \times \mathbf{S}_j$ when the symmetry is low enough^{35–37}.

In short, the position operator \mathbf{r} has two types of finite matrix elements in the tight-binding formalism. The KNB type $\langle i, \alpha | \mathbf{r} | j, \beta \rangle$ for ions $i \neq j$ (typically one TM ion and one ligand) with orbitals α and β , and the lattice type $\langle i, \alpha | \mathbf{r} | i, \beta \rangle = \mathbf{r}_i \delta_{\alpha, \beta}$ where \mathbf{r}_i is the position of ion i . If combined with first-principle calculations to accurately evaluate the $\langle i, \alpha | \mathbf{r} | j, \beta \rangle$ integrals, the ME effect in Kitaev materials and other d^5 Mott insulators can be evaluated from our results.

This paper is organized as follows. First, in Sec. II, we introduce the Hamiltonians. In Sec. III, we derive the allowed ME couplings using a symmetry group approach. In addition, we stress the importance of SOC in Sec. IV. In Sec. V, we define two different electronic mechanisms for the polarization starting from the usual LCAO (linear combination of atomic orbitals) approximation of the tight-binding model. We then explicitly consider the mechanisms in Sec. VI in the edge- and corner-sharing geometries for large SOC. Finally, we discuss our findings and conclude in Sec. VII.

II. MODEL

We consider Mott insulators with unfilled t_{2g} orbitals under an octahedral crystal field (CF) of chalcogens or halogens, which strongly split the t_{2g} and e_g orbitals. In the d^5 configuration, there is one hole in the t_{2g} orbitals per site. Accordingly, we consider a three-band Hubbard model for the holes on the lattice of TM ions, with a filling corresponding to one hole per site,

$$\mathcal{H} = \mathcal{H}_{\text{hop}} + \mathcal{H}_{\text{ion}} + \mathcal{H}_{\text{int}}, \quad (1)$$

which is the sum of a hopping, on-site, and interaction Hamiltonian, respectively. Because we are interested in bonds made of two neighboring TM ions, it is enough to consider only two sites. The Hamiltonians are concisely expressed by using the hole operators

$$\mathbf{c}_i^\dagger = (c_{i,yz,\uparrow}^\dagger, c_{i,yz,\downarrow}^\dagger, c_{i,xz,\uparrow}^\dagger, c_{i,xz,\downarrow}^\dagger, c_{i,xy,\uparrow}^\dagger, c_{i,xy,\downarrow}^\dagger). \quad (2)$$

States with doubly occupied sites (thereafter called polar states) are affected by the Coulomb interaction and Hund's coupling as described by the Kanamori Hamiltonian^{38,39} with intra orbital Coulomb repulsion U , inter-orbital repulsion $U' = U - 2J_H$, and Hund's coupling J_H ,

$$\begin{aligned} \mathcal{H}_{\text{int}} = & U \sum_{i,a} n_{i,a,\uparrow} n_{i,a,\downarrow} + (U' - J_H) \sum_{i,a < b, \sigma} n_{i,a,\sigma} n_{i,b,\sigma} \\ & + U'_{i,a \neq b} n_{i,a,\uparrow} n_{i,b,\downarrow} - J_H \sum_{i,a \neq b} c_{i,a,\uparrow}^\dagger c_{i,a,\downarrow} c_{i,b,\downarrow}^\dagger c_{i,b,\uparrow} \\ & + J_H \sum_{i,a \neq b} c_{i,a,\uparrow}^\dagger c_{i,a,\downarrow}^\dagger c_{i,b,\downarrow} c_{i,b,\uparrow}. \end{aligned} \quad (3)$$

Each hole can jump onto the filled p^6 orbitals of the ligands at a cost Δ_{pd} , the charge-transfer energy. Additionally, direct hopping between TM ions are also possible. We consider the limit where $\Delta_{pd} \gg U$, i.e., the system is in a Mott insulating phase (in contrast with the charge-transfer insulator), so that intermediate states with unfilled p orbitals can be integrated out to give the effective Hamiltonian (1). Moreover, in this limit, intermediate states with two or more unfilled p orbitals are neglected and the effective hopping integrals are simply obtained by considering the different TM-L-TM hopping processes through each ligand (L) separately. Summing the contributions from all ligands, we obtain

$$\mathcal{H}_{\text{hop}} = - \sum_{\langle ij \rangle} \mathbf{c}_i^\dagger (\hat{T}_{ij} \otimes \mathbb{I}_{2 \times 2}) \mathbf{c}_j, \quad (4)$$

where \hat{T}_{ij} is the hopping matrix between sites i and j ,

$$T_{ij}^{\alpha\beta} = t_{ij}^{\alpha\beta} + \sum_p \sum_{\gamma=x,y,z} \frac{t_{ip}^{\alpha\gamma} t_{jp}^{\beta\gamma}}{\Delta_{pd}}. \quad (5)$$

Here $t_{ij}^{\alpha\beta}$ is the hopping between the two TM ions at sites i and j with respective orbitals α and β , p labels the

ligands between the two TM ions, γ labels their orbitals, and $t_{ip}^{\alpha\gamma}$ is the hopping between the TM ion i and ligand p with orbitals α and γ , respectively. The different hopping amplitudes are the usual Slater-Koster integrals⁴⁰.

Finally, the on-site six-dimensional Hilbert space is further split by \mathcal{H}_{ion} . Each hole has an effective $L = 1$ orbital angular momentum in addition to its spin-1/2 angular momentum. The on-site Hamiltonian consists of SOC,

$$\mathcal{H}_{\text{SOC}} = \frac{\lambda}{2} \sum_{i,a} \mathbf{c}_i^\dagger (L^a \otimes \sigma^a) \mathbf{c}_i \quad (6)$$

with $\lambda > 0$, and additional CF splitting,

$$\mathcal{H}_{\text{CF}} = \Delta \sum_i \mathbf{c}_i^\dagger [(\mathbf{L} \cdot \hat{\mathbf{n}}_{\text{CF}})^2 \otimes \mathbb{I}_{2 \times 2}] \mathbf{c}_i, \quad (7)$$

so that $\mathcal{H}_{\text{ion}} = \mathcal{H}_{\text{SOC}} + \mathcal{H}_{\text{CF}}$. Here, $(L^a)_{bc} = -i\epsilon_{abc}$ and σ^a are the Pauli matrices. The unit vector $\hat{\mathbf{n}}_{\text{CF}}$ depends on the system considered. In this paper, only the trigonal ($\hat{\mathbf{n}}_{\text{CF}} = [111]$) and tetragonal ($\hat{\mathbf{n}}_{\text{CF}} = [001]$) distortions are explicitly considered in the edge-sharing and corner-sharing geometries, respectively. They correspond (up to a constant) to

$$\mathbf{L}_{[111]}^2 = -\frac{1}{3} \begin{pmatrix} 0 & 1 & 1 \\ 1 & 0 & 1 \\ 1 & 1 & 0 \end{pmatrix} \quad \text{and} \quad \mathbf{L}_{[001]}^2 = \begin{pmatrix} 1 & 0 & 0 \\ 0 & 1 & 0 \\ 0 & 0 & 0 \end{pmatrix}. \quad (8)$$

The SOC Hamiltonian splits the t_{2g} orbitals into states with total effective angular momentum $J = 1/2$ and $J = 3/2$ with energies $-\lambda$ and $\lambda/2$, respectively. The CF distortion by itself also splits the three t_{2g} states into a b_{2g} state and two e_g states. Generally, the combination of SOC and CF splits the states into three Kramers doublets.

We consider the situation where pseudospin-1/2 variables can safely be defined. This implies that the ground state is a doublet (always the case with $\lambda > 0$) that is sufficiently gapped from the other four states; it should be larger than the magnetic scale t_{eff}^2/U . (Here t_{eff} refers generally to the amplitude of the effective hopping between neighboring TM sites.) In the next section, we consider the allowed ME couplings on a symmetry basis, and do not make additional assumptions for the on-site Hamiltonian. In Sec. VI, when explicitly considering the microscopic mechanisms, we will make the assumption that SOC is large, $\lambda \gg t_{\text{eff}}^2/U$. Moreover, the additional CF distortion, whose main effect is to lower the symmetry, will be introduced perturbatively in analytical calculations. This situation is particularly relevant for late TM ions such as Ir, Os, Rh, and Ru⁴¹.

In this limit, the present model on the two-dimensional honeycomb lattice (with edge-sharing bonds, see Fig. 2) has been discussed extensively^{42–49} in the context of Kitaev materials such as α -RuCl₃^{50,51} and ‘Kitaev iridates’ A₂IrO₃ with A=Na, Li^{52,53}. The model on the square lattice (with corner-sharing bonds) has been discussed in the context of iridates or rhodates compounds such as Sr₂IrO₄ and Sr₂Ir_{1-x}Rh_xO₄⁵⁴.

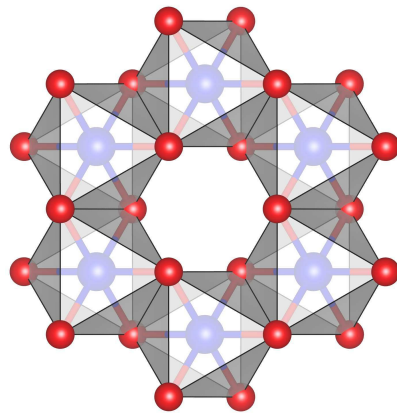


FIG. 2. Crystal structure of Kitaev materials. The blue spheres are the TM ions (Ir or Ru) and the red spheres are the ligand (O or Cl). Each TM-TM bond is in the edge-sharing geometry.

III. SYMMETRY CONSIDERATIONS

Group theory is a powerful tool to derive the allowed spin-polarization coupling^{35–37}. Here we explicitly consider the two geometries depicted in Fig. 1 with and without the inclusion of CF distortions.

In the ground state manifold (one pseudospin 1/2 per TM ion), because of the time-reversal and inversion symmetry, the general form of the coupling between the electric polarization and the pseudospins (referred to as simply spins from now on) for a given bond $\langle ij \rangle$ is $\mathbf{P} = \hat{m}(\mathbf{S}_i \times \mathbf{S}_j)$, or

$$\begin{pmatrix} P_x \\ P_y \\ P_z \end{pmatrix} = \begin{pmatrix} m_{xx} & m_{xy} & m_{xz} \\ m_{yx} & m_{yy} & m_{yz} \\ m_{zx} & m_{zy} & m_{zz} \end{pmatrix} \begin{pmatrix} (\mathbf{S}_i \times \mathbf{S}_j)_x \\ (\mathbf{S}_i \times \mathbf{S}_j)_y \\ (\mathbf{S}_i \times \mathbf{S}_j)_z \end{pmatrix}. \quad (9)$$

For a bond in the x direction, the KNB coupling corresponds to the case $m_{yz} = -m_{zy}$ and all other components equal to zero. In general, the allowed matrix elements of \hat{m} are dictated by the symmetry group of the bond $\langle ij \rangle$.

A. Edge-sharing geometry

Let us first consider the situation where each TM ion is surrounded by six ligands forming edge-sharing octahedra: Neighboring TM ions share two ligands each forming a $\phi = 90^\circ$ TM-L-TM bond as depicted in Fig. 1(b).

1. Full octahedral symmetry

Ideally, the ligands form a perfect octahedra around each TM ion in the $\pm\hat{\mathbf{x}}$, $\pm\hat{\mathbf{y}}$ and $\pm\hat{\mathbf{z}}$ directions, in which case the point group of the system is O_h . Let us consider a bond in the in the $(\hat{\mathbf{x}} - \hat{\mathbf{y}})/\sqrt{2}$ direction (also called a

Z bond). The other bonds in the honeycomb lattice of Fig. 2 are simply related by cyclic permutations.

The structure has three C_2 symmetries along the $\hat{\mathbf{u}} = (\hat{\mathbf{x}} - \hat{\mathbf{y}})/\sqrt{2}$, $\hat{\mathbf{v}} = (\hat{\mathbf{x}} + \hat{\mathbf{y}})/\sqrt{2}$ and $\hat{\mathbf{w}} = \hat{\mathbf{z}}$ axis. The symmetry group is thus D_{2h} . The character table D_{2h} is shown in Table IV of Appendix C along with the character tables of other relevant groups.

The T_2 representation of O breaks into three different irreducible representations of D_{2h} : $T_2 \rightarrow B_1 \oplus B_2 \oplus B_3$ for the three d_{ab} orbitals where a and b correspond to the $\hat{\mathbf{u}}$, $\hat{\mathbf{v}}$, and $\hat{\mathbf{w}}$ directions. The effective hopping (after integrating out the ligand) between the t_{2g} orbitals of sites i and j therefore must be

$$\hat{T}_Z(D_{2h}) = \begin{pmatrix} t_{11} & 0 & 0 \\ 0 & t_{22} & 0 \\ 0 & 0 & t_{33} \end{pmatrix}_{\mathcal{B}', \mathcal{B}'} = \begin{pmatrix} t_1 & t_2 & 0 \\ t_2 & t_1 & 0 \\ 0 & 0 & t_3 \end{pmatrix}_{\mathcal{B}, \mathcal{B}}, \quad (10)$$

where \mathcal{B} and \mathcal{B}' are the $\{\hat{\mathbf{x}}, \hat{\mathbf{y}}, \hat{\mathbf{z}}\}$ and $\{\hat{\mathbf{u}}, \hat{\mathbf{v}}, \hat{\mathbf{w}}\}$ bases, respectively. The hopping integrals can be expressed via the Slater-Koster integrals^{40,45} ($t_{pd\sigma}, t_{pd\pi}, t_{dd\sigma}, t_{dd\pi}$ and $t_{dd\delta}$),

$$\begin{aligned} t_1 &= \frac{t_{dd\pi} + t_{dd\delta}}{2}, \\ t_2 &= \frac{-t_{dd\pi} + t_{dd\delta}}{2} + \frac{t_{pd\pi}^2}{\Delta_{pd}}, \\ t_3 &= \frac{3t_{dd\sigma} + t_{dd\delta}}{4}. \end{aligned} \quad (11)$$

The spin operators $\mathbf{S} \cdot \hat{\mathbf{u}}$, $\mathbf{S} \cdot \hat{\mathbf{v}}$, and $\mathbf{S} \cdot \hat{\mathbf{w}}$ transform as $B_{1,g}$, $B_{2,g}$, and $B_{3,g}$, respectively, and the antisymmetrization between site i and j from the cross product acts as an extra $B_{1,u}$. The polarization P_α simply acts as a vector: $B_{\alpha,u}$. Hence, only two independent coupling constants are allowed,

$$\hat{m}(D_{2h}) = \begin{pmatrix} 0 & 0 & 0 \\ 0 & 0 & m_4 \\ 0 & m_5 & 0 \end{pmatrix}_{\mathcal{B}', \mathcal{B}'}. \quad (12)$$

Note that unlike the hopping matrix, which is symmetric, the spin-polarization coupling matrix does not have to be symmetric nor antisymmetric. Already, this is more general than the $\mathbf{P} \propto \hat{\mathbf{e}}_{ij} \times (\mathbf{S}_i \times \mathbf{S}_j)$ coupling, as m_4 and m_5 are *a priori* not related.

2. With trigonal distortion

Real materials have additional distortions away from the octahedral CF. For Kitaev materials, the most commonly considered distortion is a uniform elongation or compression perpendicular to the plane containing the honeycomb lattice, along the $(\hat{\mathbf{x}} + \hat{\mathbf{y}} + \hat{\mathbf{z}})/\sqrt{3}$ axis. In this case, the C_3 symmetry is intact and the point group of the system is D_{3d} . The symmetry group of the bond is

then reduced to $D_{2h} \rightarrow C_{2h}$. Its character table is shown in Table V of Appendix C.

In this case, the hopping matrix has one additional allowed term,

$$\hat{T}_Z(C_{2h}) = \begin{pmatrix} t_{11} & 0 & 0 \\ 0 & t_{22} & t_{23} \\ 0 & t_{23} & t_{33} \end{pmatrix}_{\mathcal{B}', \mathcal{B}'} = \begin{pmatrix} t_1 & t_2 & t_4 \\ t_2 & t_1 & t_4 \\ t_4 & t_4 & t_3 \end{pmatrix}_{\mathcal{B}, \mathcal{B}}, \quad (13)$$

Similarly, in the C_{2h} symmetry there are five allowed coupling constants between the spin antisymmetric vector and the polarization:

$$\hat{m}(C_{2h}) = \begin{pmatrix} m_1 & 0 & 0 \\ 0 & m_2 & m_4 \\ 0 & m_5 & m_3 \end{pmatrix}_{\mathcal{B}', \mathcal{B}'}. \quad (14)$$

3. Additional distortions

In addition to the trigonal distortion, a monoclinic distortion is also usually observed, albeit small. It further lowers the symmetry group of the bond, $C_{2h} \rightarrow C_i$. In this a case, there are no constraints; the hopping matrix has six independent terms and the matrix \hat{m} has nine. However we will not consider this symmetry situation in the following, and limit ourselves to the trigonal distortion.

A particular distortion is worth mentioning: when, for each bond, the two ligands move toward or away from the center of the bond, in the $\pm\hat{\mathbf{v}}$ direction. In principle, the bond has a C_{2h} symmetry in this case. However, the microscopic processes we consider are derived in the subsystem including only the two TM ions and two ligands. Because the displacement of the ligands is along the $\hat{\mathbf{v}}$ axis, one of the C_2 axes, the processes will only yield coupling consistent with the D_{2h} symmetry group. In a sense, this is the most practical way to study the TM-L-TM angle dependence away from the ideal $\phi = 90^\circ$ bond geometry. This case is explicitly considered in Appendix A.

B. Corner-sharing geometry

In the corner-sharing geometry, the octahedral complexes of two neighboring TM ions share one ligand. When an angle is introduced away from $\varphi = 180^\circ$, the bond inversion symmetry is broken and additional couplings are possible, deviating from Eq. (9). The $\varphi \neq 180^\circ$ geometry is considered in Appendix B.

1. Full octahedral symmetry

A bond consists of two octahedra connected along, say, the $\hat{\mathbf{x}}$ direction as depicted in Fig. 1(a). The structure

has four C_2 axes, in addition to one C_4 axis and inversion symmetry. The symmetry group is thus D_{4h} and its character table is shown in Table VI. The T_2 representation of O breaks into three different irreducible representations of D_{4h} : $T_2 \rightarrow B_2 \oplus E$ for the three t_{2g} orbitals. The d_{yz} orbital transforms as B_{2g} , while (d_{xy}, d_{xz}) transforms as E_g . The effective hopping (after integrating out the ligand) between the t_{2g} orbitals of sites i and j therefore must be

$$\hat{T}_x(D_{4h}) = \begin{pmatrix} t_1 & 0 & 0 \\ 0 & t_2 & 0 \\ 0 & 0 & t_2 \end{pmatrix}_{\mathcal{B},\mathcal{B}}. \quad (15)$$

Neglecting the d - d direct hopping, which is safe in the present geometry, we have $t_1 = 0$ and $t_2 = -\frac{t_{pd}^2}{\Delta_{pd}} \equiv t$.

The ME coupling is

$$\hat{m}_x(D_{4h}) = \begin{pmatrix} 0 & 0 & 0 \\ 0 & 0 & m_1 \\ 0 & -m_1 & 0 \end{pmatrix}_{\mathcal{B},\mathcal{B}}. \quad (16)$$

which corresponds to the KNB formula because of the high symmetry of the system (in contrast to the edge-sharing geometry).

2. Tetragonal distortion

A uniform tetragonal distortion only affects the ligands above and below the TM ions. It reduces the bond symmetry from D_{4h} to D_{2h} . Equation (16) thus becomes similar to Eq. (12) and allows a deviation from the KNB form,

$$\hat{m}_x(D_{2h}) = \begin{pmatrix} 0 & 0 & 0 \\ 0 & 0 & m_1 \\ 0 & m_2 & 0 \end{pmatrix}_{\mathcal{B},\mathcal{B}}. \quad (17)$$

The hopping processes, however, are not affected by the ligand in the $\pm\hat{z}$ direction and thus by the tetragonal distortion.

IV. IMPORTANCE OF SPIN-ORBIT COUPLING

There are two potential origins for the coupling between spin and charge (or polarization) of the electrons.

The intrinsic Pauli exclusion principle prevents two electrons with the same magnetic state to be on the same site. Alternatively, SOC explicitly couples the motion of an electron with its spin. Here, we show that SOC is actually essential in order to have a finite electronic ME coupling involving pairs of spin-1/2 operators in systems with inversion symmetry.

Without SOC, the orbital degeneracy is only lifted by the CF distortion and the pseudospins of the ground

state manifold are the original spins of the holes. Due to inversion symmetry, the polarization operator $\mathbf{P} = \hat{m}(\mathbf{S}_i \times \mathbf{S}_j)$ only has finite matrix elements between the singlet and triplets in spin space. The microscopic operator \mathbf{P} is obviously trivial in terms of electronic spin operators. Therefore, the effective polarization operator in the ground state manifold vanishes without SOC. This argument is only valid when the symmetry group of the bond contains inversion symmetry, without which spin-symmetric matrix elements (i.e., triplet to triplet or singlet to singlet) are possible.

To understand better the role of SOC, we consider the localized single-hole wave functions in the ground state. If we now consider a single bond $\langle ij \rangle$, each wave function transforms as a representation, say Γ , of the bond symmetry group. Without SOC, Γ is one-dimensional with an extra spin degeneracy. With SOC, however, Γ is a two-dimensional representation of the corresponding spin double group that mixes orbitals and spins.

Because the wave functions are on different sites, there is an extra site index. For two sites, this extra degree of freedom transforms as one of two different one-dimensional representations of the bond symmetry group so that the two-hole state is overall odd under exchange (as imposed by the fermionic statistic): either $\Gamma_{\text{sym}} = 1$, the trivial representation, or Γ_{antisym} . The explicit identification of Γ_{antisym} depends on the group (see, e.g., the tables in Appendix C, where it is indicated as “i-j antisym”), but it is always odd under inversion symmetry.

Without SOC, $\Gamma \otimes \Gamma = 1$ and, due to the extra spin degeneracy (singlet or triplet), the full two-hole ground state manifold transforms as $\Gamma_{\text{sym}} \oplus \Gamma_{\text{antisym}}$. Because the polarization is odd under inversion, only matrix elements between spin triplet and spin singlet are possible when SOC is absent, which, as already mentioned, cannot be finite. Once SOC is introduced, each irreducible representation of $\Gamma \otimes \Gamma = \sum_k \Gamma_k$ is either even or odd under permutation of the single-hole wave functions, and has to be combined accordingly with Γ_{sym} or Γ_{antisym} . However, the dichotomy does not correspond to spin triplet and spin singlet anymore, and the above argument cannot be used.

V. POLARIZATION

We start by defining the polarization operator \mathbf{P} in second quantized notation. This is done by explicitly calculating its matrix elements between the different single-electron wave functions. In this section, the spin degree of freedom is not important and not written explicitly. The Bloch wave functions can be expressed as

$$\psi_m(\mathbf{k}, \mathbf{r}) = \frac{1}{N} \sum_n a_m(\mathbf{R}_n, r) e^{i\mathbf{k}\cdot\mathbf{r}}, \quad (18)$$

where \mathbf{R}_n are lattice vectors, N is the number of unit cells and $a_m(\mathbf{R}_n, r)$ is a Wannier function for the unit

cells at \mathbf{R}_n . In the tight-binding approach, the LCAO approximation is used for which the exact Wannier functions are replaced by isolated atomic orbitals (or a linear combination of them, when there are multiple atoms per unit cell).

We now consider a single TM-TM bond consisting of two TM ions at positions \mathbf{r}_1^{TM} and \mathbf{r}_2^{TM} and M ligands at positions \mathbf{r}_p^{L} ($p = 1, \dots, M$). There are thus $10 + 3M$ different atomic orbitals centered at $2 + M$ different positions,

$$\psi_{\text{at}}(\mathbf{r}) = \begin{cases} \psi_{\alpha}(\mathbf{r} - \mathbf{r}_1^{\text{TM}}), & \psi_{\alpha}(\mathbf{r} - \mathbf{r}_2^{\text{TM}}) & (d \text{ orbitals}) \\ \psi_{\gamma}(\mathbf{r} - \mathbf{r}_p^{\text{L}}) & p = 1, \dots, M & (p \text{ orbitals}) \end{cases}, \quad (19)$$

where $\alpha \in \{yz, xz, xy, x^2 - y^2, 3z^2 - r^2\}$, and $\gamma \in \{x, y, z\}$. We furthermore assume, for simplicity, that the atomic orbitals are orthogonal to each other. The different atomic orbitals are written as $|\mathbf{R}, \alpha\rangle$, where \mathbf{R} is the position of the corresponding ion and α labels the orbital. The polarization operators $\mathbf{P} = e\mathbf{r}$ is then obtained by calculating the different matrix elements $e \langle \mathbf{R}, \alpha | \mathbf{r} | \mathbf{R}', \beta \rangle$. In the following, we set the elementary charge $e = 1$. In general, \mathbf{P} can be decomposed into single-site terms ($\mathbf{R} = \mathbf{R}'$) and two-site terms ($\mathbf{R} \neq \mathbf{R}'$), which we call ‘‘lattice polarization’’ and ‘‘hopping polarization’’, respectively.

A. Lattice polarization

First, for a given ion, the matrix elements are given by

$$\langle \mathbf{R}, \alpha | \mathbf{r} | \mathbf{R}, \beta \rangle = \mathbf{R} \delta_{\alpha\beta} + \langle \mathbf{0}, \alpha | \mathbf{r} | \mathbf{0}, \beta \rangle = \mathbf{R} \delta_{\alpha\beta}. \quad (20)$$

Indeed, the product of two d or two p orbitals is even under inversion symmetry. This defines the lattice polarization, which reads $\sum_i \mathbf{r}_i n_i$, where $n_i = \sum_{\alpha} n_{i,\alpha} = \sum_{\alpha} c_{i,\alpha}^{\dagger} c_{i,\alpha}$ for the ion at position \mathbf{r}_i (both ligands and TM ions). Moreover, the Mott insulator is overall neutral and has a fixed number of electrons on each equivalent site in the ground state manifold: n_{TM} (n_{L}) for TM ions (ligands). The lattice polarization is

$$\mathbf{P}_{\text{lat}} = \sum_{i \in \text{TM}} \mathbf{r}_i^{\text{TM}} \delta n_i + \sum_{p \in \text{L}} \mathbf{r}_p^{\text{L}} \delta n_p \quad (21)$$

where $\delta n_i = n_i - n_{\text{TM(L)}}$ for TM ions (ligands). This contribution is intrinsic to the tight-binding model. It is directly related to the ‘‘Hubbard current’’ that we obtain at first order in the vector potential from the Peierls substitution in the hopping integrals. In the Mott insulating phase, it arises from virtual hopping between neighboring atoms when t/U is finite, so that the ground states are not exact magnetic states but contain a small mixture of polar states. After integrating out the p -orbital intermediate states, we are left with two types of contributions at the lowest order in t/U : the contribution from the TM ions and from the ligands [first and second term

in Eq. (21)]. For a TM-TM pair $\langle ij \rangle$, the contribution from the TM ions is

$$\mathbf{P}_{\text{lat}, \langle ij \rangle, \text{eff}}^{(\text{TM})} = \mathbb{P} \left[\mathcal{H}_{\text{hop}}^{ij} \frac{\mathbb{Q}_j}{(E_0 - \mathcal{H}_0)^2} \mathcal{H}_{\text{hop}}^{ji} - \mathcal{H}_{\text{hop}}^{ji} \frac{\mathbb{Q}_i}{(E_0 - \mathcal{H}_0)^2} \mathcal{H}_{\text{hop}}^{ij} \right] \mathbb{P} \mathbf{a}_{ij}, \quad (22)$$

where \mathbb{P} and \mathbb{Q}_k are the projection operators on the ground state manifold (with energy E_0) and polar states with double occupancy at site k , respectively. \mathcal{H}_0 is the local Hamiltonian (without hopping), $\mathcal{H}_{\text{hop}}^{ij}$ is the effective hopping Hamiltonian between sites i and j , and $\mathbf{a}_{ij} = \mathbf{r}_j^{\text{TM}} - \mathbf{r}_i^{\text{TM}}$, whose norm is a , the lattice spacing. This operator scales as t_{eff}^2/U^2 or $t_{pd}^4/(\Delta_{pd}^2 U^2)$. Here t_{pd} generally denotes the TM-L hopping integrals.

The contribution from the ligands comes when we apply \mathbf{P} on a polar state with a hole on a ligand. After integrating out the intermediate states, the operator takes the form of an effective hopping,

$$\mathbf{P}_{\text{lat}, \langle ij \rangle}^{(\text{L})} = \sum_p \sum_{\gamma=x,y,z} \frac{t_{ip}^{\alpha\gamma} t_{jp}^{\beta\gamma}}{\Delta_{pd}^2} \mathbf{r}_p^{\text{L}} \left(c_{i,\alpha}^{\dagger} c_{j,\beta} + c_{j,\beta}^{\dagger} c_{i,\alpha} \right), \quad (23)$$

where p labels the ligands between the two TM ions at positions \mathbf{r}_p^{L} and γ labels their orbitals. This operators scales as t_{pd}^2/Δ_{pd}^2 and its projection onto the ground state manifold is

$$\mathbf{P}_{\text{lat}, \langle ij \rangle, \text{eff}}^{(\text{L})} = \mathbb{P} \left[\mathbf{P}_{\text{lat}, ij}^{(\text{L})} \frac{\mathbb{Q}_j}{E_0 - \mathcal{H}_0} \mathcal{H}_{\text{hop}}^{ji} + \mathbf{P}_{\text{lat}, ji}^{(\text{L})} \frac{\mathbb{Q}_i}{E_0 - \mathcal{H}_0} \mathcal{H}_{\text{hop}}^{ij} \right] \mathbb{P} + \text{H.c.}, \quad (24)$$

which, unlike the contributions from TM ions, scales as $t_{pd}^2 t_{\text{eff}}/(\Delta_{pd}^2 U)$ or $t_{pd}^4/(\Delta_{pd}^3 U)$ and is thus smaller by a factor of U/Δ_{pd} .

B. Hopping polarization

The remaining matrix elements are

$$\langle \mathbf{R}, \alpha | \mathbf{r} | \mathbf{R}', \beta \rangle = \langle \mathbf{R}, \alpha | \mathbf{r} - \mathbf{r}_0 | \mathbf{R}', \beta \rangle = \left\langle -\frac{\mathbf{d}}{2}, \alpha \left| \mathbf{r} \right| \frac{\mathbf{d}}{2}, \beta \right\rangle \quad (25)$$

where $\mathbf{R} \neq \mathbf{R}'$, $\mathbf{r}_0 = (\mathbf{R} + \mathbf{R}')/2$ and $\mathbf{d} = \mathbf{R}' - \mathbf{R}$ is the vector separating the two ions: either TM-TM (in which case $\|\mathbf{d}\| = a$) or TM-L. Anticipating the integrating out of the p -orbital states, we only consider the d - d and the p - d polarization integrals. The behavior under inversion symmetry implies that $\langle \mathbf{R}, \alpha | \mathbf{r} | \mathbf{R}', \gamma \rangle = \langle \mathbf{R}, \gamma | \mathbf{r} | \mathbf{R}', \alpha \rangle$ for a p - d integral and that $\langle \mathbf{R}, \alpha | \mathbf{r} | \mathbf{R}', \beta \rangle = -\langle \mathbf{R}, \beta | \mathbf{r} | \mathbf{R}', \alpha \rangle$ for a d - d integral.

After integrating out the intermediate states, we have

$$\mathbf{P}_{\text{hop}} = \sum_{\langle i,j \rangle} \sum_{\alpha, \beta} \mathbf{p}_{ij}(\alpha, \beta) \left(c_{i,\alpha}^{\dagger} c_{j,\beta} + c_{j,\beta}^{\dagger} c_{i,\alpha} \right), \quad (26)$$

where $\mathbf{p}_{ij}(\alpha, \beta)$ is the effective polarization integral between the TM ions at site i and j with orbitals α and β , respectively. The projection onto the ground state manifold is obtained similarly to Eq. (24).

There are two contributions to $\mathbf{p}_{ij}(\alpha, \beta)$: one from direct d - d polarization integrals, and a TM-L-TM superexchange-like contribution from p - d integrals, so that

$$\mathbf{p}_{ij}(\alpha, \beta) = \langle \mathbf{r}_i^{\text{TM}}, \alpha | \mathbf{r} | \mathbf{r}_j^{\text{TM}}, \beta \rangle + \sum_p \sum_{\gamma=x,y,z} \frac{\langle \mathbf{r}_i^{\text{TM}}, \alpha | \mathbf{r} | \mathbf{r}_p^{\text{L}}, \gamma \rangle t_{jp}^{\beta\gamma} + t_{ip}^{\alpha\gamma} \langle \mathbf{r}_p^{\text{L}}, \gamma | \mathbf{r} | \mathbf{r}_j^{\text{TM}}, \beta \rangle}{\Delta_{pd}}, \quad (27)$$

where p labels the ligands between the two TM ions and γ their orbitals.

Such integrals between d and p orbitals were used in the original KNB derivation¹⁶. However, in the KNB formalism the integrals are only considered at zeroth order in the interatomic distance (i.e., with $\mathbf{r}_i^{\text{TM}} = \mathbf{r}_j^{\text{TM}}$). The outcome of this approximation is that, the finite integrals involving t_{2g} orbitals, $\langle p_z | y | d_{yz} \rangle$ and its six permutations, are all equal to each other.

In the following, we derive a more complete scheme to calculate the different integrals for any vector \mathbf{d} separating two ions, in a manner that is reminiscent of the Slater-Koster hopping integrals⁴⁰. We find five different symmetry-allowed integrals for a p - d pair, and only two for a d - d pair.

To summarize, we have two different mechanisms. The lattice polarization has a contribution from the TM ions, which scales as $a \cdot t_{pd}^4 / (\Delta_{pd}^2 U^2)$, and a contribution from the ligands, which scales as $a \cdot t_{pd}^4 / (\Delta_{pd}^3 U)$. In the magnetic ground state manifold, the hopping polarization is obtained after one additional virtual hopping and thus scale as $p_{\text{eff}} t_{\text{eff}} / U$ [where p_{eff} generally represents the effective hopping polarization between two TM sites defined by Eq. (27)]. In terms of p - d integrals, the scaling is $p_{pd} t_{pd}^3 / (\Delta_{pd}^2 U)$. Therefore, in the Mott insulating limit where $\Delta_{pd} \gg U$, the dominant contribution is determined by comparing p_{eff} with $a \cdot t_{\text{eff}} / U$, or by directly comparing p_{pd} with $a \cdot t_{pd} / U$ if the p - d integrals are dominant.

C. Polarization integrals

The integrals in Eq. (26) are two-center integrals with an extra $l = 1$ spherical harmonic at the middle point. A p orbital can be expressed as a linear combination of $p\sigma$ and $p\pi_{\pm}$ functions with respect to the axis \mathbf{d} along the bond, and a d orbital can be expressed as a combination of $d\sigma$, $d\pi_{\pm}$, and $d\delta_{\pm}$ functions. Here σ , π_{\pm} , and δ_{\pm} refer to the component of angular momentum along the axis. The different labels directly correspond to the cubic harmonics as shown in Table I. For p - d integrals, five symmetry channels are allowed. They can be separated into longitudinal (\mathbf{P} along the bond) and transverse (\mathbf{P}

x	y	z	yz	xz	xy	$\frac{x^2-y^2}{2}$	$\frac{3z^2-r^2}{2\sqrt{3}}$
π_+	π_-	σ	π_-	π_+	δ_+	δ_-	σ

TABLE I. Cubic harmonics of p and d orbitals expressed with respect to their component of angular momentum along the z axis.

orthogonal to the bond) components. To lighten the notation, the center of the atomic orbitals is omitted and assumed to be $-\mathbf{d}/2$ ($\mathbf{d}/2$) for the bra (ket) state. The two longitudinal integrals are

$$P_{pd\sigma}^{\parallel} = \langle p\sigma | \sigma | d\sigma \rangle \quad (28)$$

$$P_{pd\pi}^{\parallel} = \langle p\pi_{\pm} | \sigma | d\pi_{\pm} \rangle \quad (29)$$

and the three transverse integrals are

$$P_{p\pi d\sigma}^{\perp} = \langle p\pi_{\pm} | \pi_{\pm} | d\sigma \rangle \quad (30)$$

$$P_{p\sigma d\pi}^{\perp} = \langle p\sigma | \pi_{\pm} | d\pi_{\pm} \rangle \quad (31)$$

$$P_{p\pi d\delta}^{\perp} = \langle p\pi_{\pm} | \pi_{\mp} | d\delta_{\pm} \rangle = \pm \langle p\pi_{\pm} | \pi_{\pm} | d\delta_{\mp} \rangle \quad (32)$$

Here σ and π_{\pm} denote the projections of \mathbf{r} on the σ and π_{\pm} axes.

For the d - d integrals, there are only two transverse components,

$$P_{d\sigma d\pi}^{\perp} = \langle d\sigma | \pi_{\pm} | d\pi_{\pm} \rangle = -\langle d\pi_{\pm} | \pi_{\pm} | d\sigma \rangle \quad (33)$$

$$P_{d\pi d\delta}^{\perp} = \langle d\pi_{\pm} | \pi_{\mp} | d\delta_{\pm} \rangle = \pm \langle d\pi_{\pm} | \pi_{\pm} | d\delta_{\mp} \rangle = -\langle d\delta_{\pm} | \pi_{\mp} | d\pi_{\pm} \rangle = \mp \langle d\delta_{\mp} | \pi_{\pm} | d\pi_{\pm} \rangle. \quad (34)$$

From those expressions, we can then calculate the polarization integrals in a fixed basis for \mathbf{d} pointing in an arbitrary direction. Using the notation of Slater and Koster⁴⁰, we denote the cosine angles of \mathbf{d} as (l, m, n) . For example we have

$$\begin{aligned} \langle p_x | x | d_{xy} \rangle &= \sqrt{3} l^3 m P_{pd\sigma}^{\parallel} + lm (1 - 2l^2) P_{pd\pi}^{\parallel} \\ &+ \sqrt{3} lm (1 - l^2) P_{p\pi d\sigma}^{\perp} + lm (1 - 2l^2) P_{p\sigma d\pi}^{\perp} \\ &- lm (1 - l^2) P_{p\pi d\delta}^{\perp}. \end{aligned} \quad (35)$$

Other integrals are found in Table VIII in Appendix D. In particular, for a bond along the z axis, the t_{2g} - p integrals of the KNB theory split into three different possible values:

$$\begin{aligned} \langle p_x | z | d_{xz} \rangle &= \langle p_y | z | d_{yz} \rangle = P_{pd\pi}^{\parallel} \\ \langle p_z | y | d_{yz} \rangle &= \langle p_z | x | d_{xz} \rangle = P_{p\sigma d\pi}^{\perp} \\ \langle p_x | y | d_{xy} \rangle &= \langle p_y | x | d_{xy} \rangle = P_{p\pi d\delta}^{\perp} \end{aligned} \quad (36)$$

In the limit where $d = \|\mathbf{d}\| \rightarrow 0$, the three integrals of Eq. (36) are identical and can be roughly calculated using the orbitals of the hydrogen like atom¹⁶. Moreover,

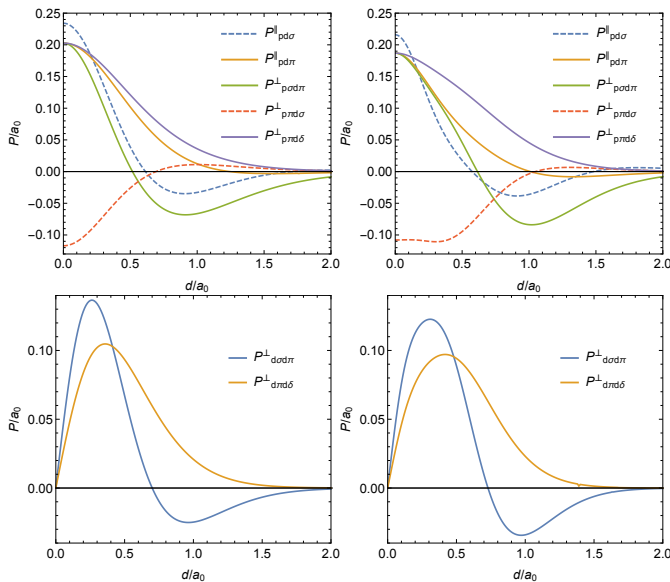


FIG. 3. The different p - d (top) and d - d (bottom) polarization integrals as a function of the atomic spacing d , in units of a_0 , the Bohr radius. The cases of chromium and oxygen atoms (left) and ruthenium and chloride atoms (right) are plotted using hydrogenlike atomic orbitals.

the d - d integrals vanish due to their behavior under inversion symmetry. The integrals have been numerically calculated as a function of the interatomic distance d using hydrogenlike atomic orbitals. The results are shown in Fig. 3. The hydrogenlike atomic orbitals of chromium ($3d$ orbitals with $Z = 24$) and oxygen ($2p$ orbitals with $Z = 8$), and of ruthenium ($4d$ orbitals with $Z = 44$) and chloride ($3p$ orbitals with $Z = 17$) have been used (left and right figures, respectively). For a typical interatomic distance of $2\text{\AA} \sim 3.8a_0$ (a_0 is the Bohr radius), the p - d integrals are considerably smaller than the zeroth order approximation used in the KNB theory by a factor of $\sim 10^{4-6}$.

It is important to note that in general, the hydrogenlike atom model is not a good approximation. In particular, when the system is close to the Mott transition, or close to a molecular-insulating regime, the wave functions might be spread over several sites with significant overlap. This is especially true for the $4d$ or $5d$ compounds considered in this paper. In such a case, the polarization integrals should be larger (as are the tight-binding hopping integrals) and first-principle methods should be used to evaluate the atomic orbitals. Nevertheless, the symmetry considerations (the classification into different symmetry channels) still apply.

VI. MICROSCOPIC MECHANISMS

We are now looking explicitly at the mechanisms behind the allowed couplings in terms of the microscopic lattice and hopping polarization defined in Sec. V. For

each allowed coupling constants m_{1-5} in Eqs. (12), (14), (16), and (17), we separate the contributions as

$$m_i = a\mathbb{A}_i + \mathbb{B}_i, \quad (37)$$

where \mathbb{A}_i and \mathbb{B}_i are the coupling constants resulting from the \mathbf{P}_{lat} and \mathbf{P}_{hop} , respectively. Here a is the lattice spacing between two TM ions so that the contributions \mathbb{A}_i are unitless, while the contributions \mathbb{B}_i have units of distance coming from the polarization integrals. The results are summarized in Table II and shown in Figs. 5 and 6 for the edge-sharing geometry, and are summarized in Table III for the corner-sharing geometry.

A. Edge-sharing geometry

In the edge-sharing geometry, the five coupling constants m_{1-5} in Eq. (14) are defined through

$$\begin{aligned} \mathbf{P}_{\text{eff}} = & m_1[\hat{\mathbf{u}} \cdot (\mathbf{S}_i \times \mathbf{S}_j)]\hat{\mathbf{u}} \\ & + [m_2 (\mathbf{S}_i \times \mathbf{S}_j) \cdot \hat{\mathbf{v}} + m_4 (\mathbf{S}_i \times \mathbf{S}_j) \cdot \hat{\mathbf{w}}]\hat{\mathbf{v}} \\ & + [m_5 (\mathbf{S}_i \times \mathbf{S}_j) \cdot \hat{\mathbf{v}} + m_3 (\mathbf{S}_i \times \mathbf{S}_j) \cdot \hat{\mathbf{w}}]\hat{\mathbf{w}}. \end{aligned} \quad (38)$$

1. Lattice polarization

In order to calculate the contribution from \mathbf{P}_{lat} in Eq. (21), we consider the subsystem made of one bond depicted in Fig. 1(b): two TM ions at sites i and j separated by $a\hat{\mathbf{u}}$, and two ligands also separated by a distance a when $\phi = 90^\circ$. All the calculations done in this section are extended to the $\phi \neq 90^\circ$ case in Appendix A. In the subsystem, $\sum_k \delta n_k = 0$ and we can choose the origin at the center of the bond. Then, the contribution from the TM ions is always in the $\hat{\mathbf{u}}$ direction, and the contribution from the ligands is perpendicular to it. Without trigonal distortion, the latter is exactly in the $\hat{\mathbf{v}}$ direction.

Without trigonal distortion, we see in Eq. (12) that from symmetry considerations, $m_1 = 0$. Hence, the contribution to \mathbf{P}_{lat} along the bond coming from the TM ions vanishes due to the high D_{2h} symmetry of the bond. More intuitively, this can be understood from the original microscopic Hamiltonian (1). With the trigonal CF $\Delta = 0$, the on-site Hamiltonian is $O(3)$ rotationally invariant because we neglect the e_g orbitals. The bond symmetry is encoded in the hopping matrix, which has three eigenvectors corresponding to the three C_2 axes of the D_{2h} group: $\hat{\mathbf{u}}$, $\hat{\mathbf{v}}$, and $\hat{\mathbf{w}}$. The on-site energy eigenstates are grouped into three Kramers pairs (or three states with a pseudospin variable). Because SOC is rotationally invariant, the hopping is completely diagonal with respect to the pseudospins. As the polarization only connects states with different parities, the contribution from $\mathbf{P}_{\text{lat}}^{(\text{TM})}$ along the bond must vanish. When $\Delta \neq 0$, the hopping is no longer diagonal with respect to the pseudospins and a finite contribution is possible.

Additionally, in the specific case where $(\hat{\mathbf{x}}+\hat{\mathbf{y}}+\hat{\mathbf{z}})/\sqrt{3}$ is an eigenvector of the hopping matrix (i.e., the CF Hamiltonian and the hopping matrix are simultaneously diagonalizable), the system recovers an accidental D_{2h} symmetry and the contribution vanishes. This happens exactly when $t_1 + t_2 - t_3 - t_4 = 0$.

The contribution to m_1 in Eq. (14) can be found numerically with exact diagonalization of the two-site system or with perturbation theory. Using perturbation theory at second order in \mathcal{H}_{hop} , as explained in Sec. V, we find a contribution to m_1 ,

$$\mathbf{P}_{\text{lat, eff}}^{(\text{TM})} = \mathbb{A}_1[\hat{\mathbf{u}} \cdot (\mathbf{S}_i \times \mathbf{S}_j)]a\hat{\mathbf{u}}. \quad (39)$$

From Eq. (22),

$$\mathbb{A}_1[\hat{\mathbf{u}} \cdot (\mathbf{S}_i \times \mathbf{S}_j)] = P_{ij} - P_{ji}, \quad (40)$$

where

$$P_{ij} = \mathbb{P}\mathcal{H}_{\text{hop}}^{ij} \frac{Q_j}{(E_0 - \mathcal{H}_0)^2} \mathcal{H}_{\text{hop}}^{ji} \mathbb{P}. \quad (41)$$

Here, $\mathcal{H}_0 = \mathcal{H}_{\text{SOC}} + \mathcal{H}_{\text{CF}} + \mathcal{H}_{\text{int}}$. Including the trigonal distortion, the calculation is too cumbersome to be performed analytically, but we can treat \mathcal{H}_{CF} as an additional perturbation. At the lowest order (second order in the hopping and first order in Δ),

$$\begin{aligned} P_{ij} = & \left[-\frac{2}{3\lambda} \mathbb{P}_{\frac{1}{2}} \mathcal{H}_{\text{hop}}^{ij} \frac{Q_j}{(E_0 - \mathcal{H}'_0)^2} \mathcal{H}_{\text{hop}}^{ji} \mathbb{P}_{\frac{3}{2}} \mathcal{H}_{\text{CF}} \mathbb{P}_{\frac{1}{2}} \right. \\ & + \mathbb{P}_{\frac{1}{2}} \mathcal{H}_{\text{hop}}^{ij} \frac{Q_j}{(E_0 - \mathcal{H}'_0)^2} \mathcal{H}_{\text{CF}} \frac{Q_j}{E_0 - \mathcal{H}'_0} \mathcal{H}_{\text{hop}}^{ji} \mathbb{P}_{\frac{1}{2}} \left. \right] \\ & + \text{H.c.}, \end{aligned} \quad (42)$$

where $\mathbb{P}_{\frac{1}{2}}$ and $\mathbb{P}_{\frac{3}{2}}$ are the projection operators on the $J = 1/2$ states and the $J = 3/2$ states, respectively. In Eq. (42), $\mathcal{H}'_0 = \mathcal{H}_{\text{SOC}} + \mathcal{H}_{\text{int}}$.

The full expression of \mathbb{A}_1 is large and given in Appendix E1. It can be written as

$$\mathbb{A}_1 = \Delta(t_1 + t_2 - t_3 - t_4) \frac{J_H}{\lambda} \times \frac{P}{Q}, \quad (43)$$

where the P and Q are polynomials given in Appendix E1. In the $U \gg J_H, \lambda$ limit, we find

$$\lim_{\substack{J_H/U \rightarrow 0 \\ \lambda/U \rightarrow 0}} \mathbb{A}_1 = \sqrt{2} \frac{64}{81} \Delta(t_1 + t_2 - t_3 - t_4)(t_1 + t_2 + t_3) \frac{J_H}{\lambda U^3}. \quad (44)$$

Interestingly, the unitless constant \mathbb{A}_1 vanishes when $J_H = 0$. This can be seen in Fig. 5(a) as well. The ME coupling in Eq. (39) was used in Ref.³⁴ to explain the subgap optical conductivity of Kitaev materials.

The calculation of \mathbb{A}_1 was also performed using perturbation exact in Δ and using exact diagonalization on a two-site system. In Fig. 4, we plot \mathbb{A}_1 calculated with the three methods: exact diagonalization, perturbation theory (quadratic in the hopping) and from Eq. (43)

(quadratic in the hopping and linear in the CF distortion). The physical parameters were set to $U = 2310$ meV, $J_H = 320$ meV, $\lambda = 140$ meV, which correspond to typical values for α -RuCl₃^{45,55}. In Figs. 4(a) and 4(b), we set $t_1 = t_3 = 0$ and calculate \mathbb{A}_1 as a function of t_2 and Δ , respectively. For α -RuCl₃, the trigonal CF distortion Δ is typically somewhere between -15 meV and -70 meV (not so small compared to λ). In Fig. 4(c), we also consider finite values for t_1 , t_3 , and t_4 , and plot exact diagonalization results for different sets of realistic values. We find that for typical values of the hopping amplitudes, the perturbation theory calculations very well reproduce the exact diagonalization calculations. Moreover, the perturbation theory linear in Δ is, in most cases, a surprisingly good approximation up to relatively large values of Δ as long as $|\Delta| < \lambda$ (which is usually the case in $4d$ and $5d$ materials due to strong SOC). Interestingly, the behavior depends considerably on the hopping integrals and their relative amplitudes. In particular, the sign of \mathbb{A}_1 changes as $|t_3/t_2|$ increases. Finally, we properly observe in Figs. 4(b) and 4(c) that both SOC and the trigonal CF are required in order have a finite \mathbf{P} along the bond. Indeed, $\mathbb{A}_1 \rightarrow 0$ for $\Delta \rightarrow \pm\infty$, which is equivalent to $\lambda \rightarrow 0$.

The second contribution to \mathbf{P}_{lat} , from the ligands, is obtained from Eq. (23) and is just the effective hopping matrix elements arising from the TM-L-TM processes, but with opposite sign for the two ligands so that the matrix is antisymmetric. Without trigonal distortion, it is oriented along $\hat{\mathbf{v}}$ so that

$$\mathbf{P}_{\text{lat}}^{(\text{L})} = \frac{t_{pd}^2}{\Delta_{pd}^2} \left[\mathbf{c}_i^\dagger \begin{pmatrix} 0 & -1 & 0 \\ 1 & 0 & 0 \\ 0 & 0 & 0 \end{pmatrix} \mathbf{c}_j + \text{H.c.} \right] \frac{a}{2} \hat{\mathbf{v}}. \quad (45)$$

Equation (45) has the same form as the hopping polarization terms considered in the next subsection. We already know from symmetry that it eventually yields

$$\begin{aligned} \mathbf{P}_{\text{lat, eff}}^{(\text{L})} = & [\mathbb{A}_2 \hat{\mathbf{v}} \cdot (\mathbf{S}_i \times \mathbf{S}_j) + \mathbb{A}_4 \hat{\mathbf{w}} \cdot (\mathbf{S}_i \times \mathbf{S}_j)]a\hat{\mathbf{v}} \\ & + [\mathbb{A}_5 \hat{\mathbf{v}} \cdot (\mathbf{S}_i \times \mathbf{S}_j) + \mathbb{A}_3 \hat{\mathbf{w}} \cdot (\mathbf{S}_i \times \mathbf{S}_j)]a\hat{\mathbf{w}}, \end{aligned} \quad (46)$$

where only $\mathbb{A}_4 \neq 0$ without trigonal CF. Furthermore, it is safe to neglect the displacement of the ligands along $\hat{\mathbf{w}}$ in which case $\mathbb{A}_5 = \mathbb{A}_3 = 0$. The constants are explicitly calculated in the next subsection.

In Fig. 5, we plot the coupling constants \mathbb{A}_1 , \mathbb{A}_2 , and \mathbb{A}_4 , calculated with exact diagonalization on a two-site cluster without any approximations, as a function of J_H , λ , and Δ in Figs. 5(a), 5(b), and 5(c), respectively. Note that we cannot decrease λ below a certain threshold in Fig. 5(b) because the pseudospin 1/2 are not well defined for $\Delta < 0$ when $\lambda = 0$ (the local ground state is fourfold degenerate).

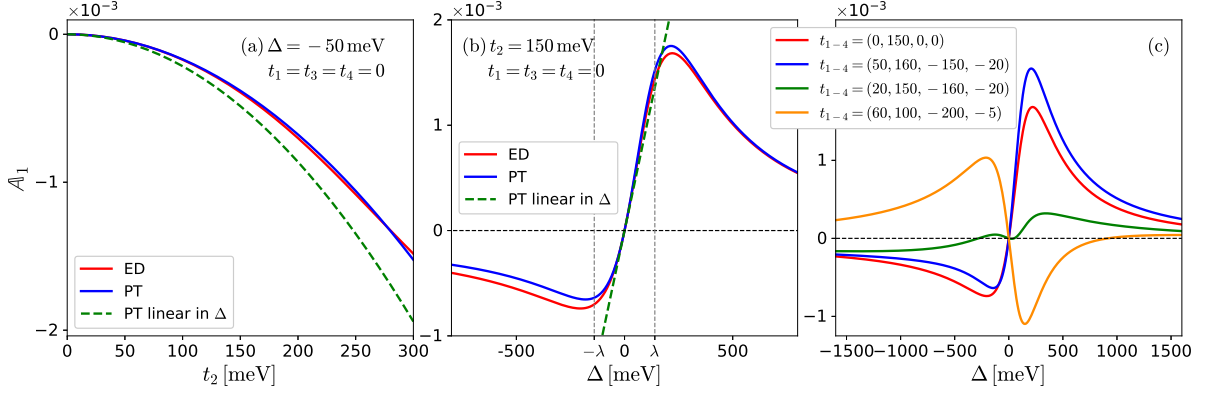


FIG. 4. Numerical evaluation of \mathbb{A}_1 in Eq. (39). Results using exact diagonalization (ED) (red line), perturbation theory (PT) exact in Δ (blue line), and perturbation theory linear in Δ (green dashed line) are plotted in (a) and (b), for typical values of the physical parameters: $U = 2310$ meV, $J_H = 320$ meV, $\lambda = 140$ meV, and we set $t_1 = t_3 = t_4 = 0$. It is plotted (a) as a function of t_2 with $\Delta = -50$ meV and (b) as a function of Δ with $t_2 = 150$ meV. (c) shows ED calculation of \mathbb{A}_1 as a function of Δ for different sets of values t_{1-4} taken from the literature^{45,55}. The values are indicated in meV units.

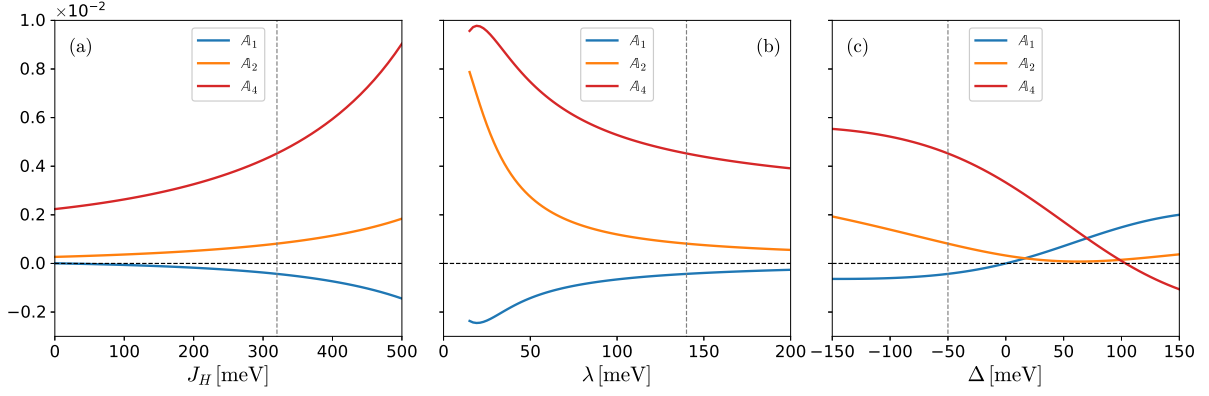


FIG. 5. Numerical evaluation of \mathbb{A}_1 , \mathbb{A}_2 , and \mathbb{A}_4 in Eqs. (37) and (45) using exact diagonalization as a function of (a) J_H , (b) λ , and (c) Δ . The nonvarying physical parameters are chosen as $U = 2310$ meV, $J_H = 320$ meV, $\lambda = 140$ meV, $\Delta = -50$ meV, $t_1 = 50$ meV, $t_2 = 160$ meV, $t_3 = -150$ meV, and $t_4 = -20$ meV, typical for α -RuCl₃.

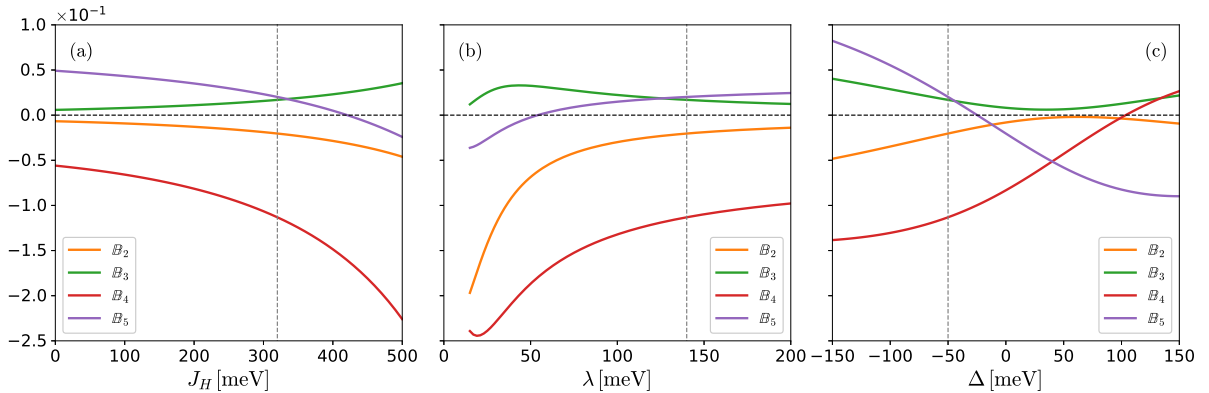


FIG. 6. Numerical evaluation of \mathbb{B}_{2-4} in Eq. (37) using exact diagonalization as a function of (a) J_H , (b) λ , and (c) Δ . The nonvarying physical parameters are chosen as $U = 2310$ meV, $J_H = 320$ meV, $\lambda = 140$ meV, $\Delta = -50$ meV, $t_1 = 50$ meV, $t_2 = 160$ meV, $t_3 = -150$ meV, and $t_4 = -20$ meV, typical for α -RuCl₃. The coupling constants are plotted in units of b_5 (see Eq. (52)) where we assumed $b_4 = -b_5$ for simplicity.

TABLE II. Coupling constants defined in Eqs. (14) and (37) for the edge-sharing geometry in the $J_H/U \rightarrow 0$ limit (and $\lambda/U \rightarrow 0$ for \mathbb{A}_1). The CF is included through \mathcal{H}_{CF} but the displacement of the ligands is neglected. The coefficients b_4 and b_5 are given in terms of the polarization integrals in Eq. (52).

$\mathbb{A}_1 = \sqrt{2} \frac{64}{81} \Delta (t_1 + t_2 - t_3 - t_4) (t_1 + t_2 + t_3) \frac{J_H}{\lambda U^3}$
$\mathbb{A}_2 = -\frac{t_{pd\pi}^2}{\Delta^2} \sqrt{2} \frac{16}{81} \Delta \frac{2t_1+t_3}{\lambda U}$
$\mathbb{A}_3 = 0$
$\mathbb{A}_4 = \frac{t_{pd\pi}^2}{\Delta^2} \left[\frac{8}{9} \frac{2t_1+t_3}{U} + \frac{64}{81} \Delta \frac{t_2+2t_4}{\lambda U} \right]$
$\mathbb{A}_5 = 0$
$\mathbb{B}_1 = 0$
$\mathbb{B}_2 = b_4 \sqrt{2} \frac{32}{81} \Delta \frac{2t_1+t_3}{\lambda U}$
$\mathbb{B}_3 = b_5 \sqrt{2} \frac{32}{81} \Delta \frac{2t_1+t_3}{\lambda U}$
$\mathbb{B}_4 = -b_4 \left[\frac{16}{9} \frac{2t_1+t_3}{U} + \frac{128}{81} \Delta \frac{t_2+2t_4}{\lambda U} \right]$
$\mathbb{B}_5 = b_5 \left[-\frac{16}{9} \frac{2t_1+t_3}{U} + \frac{32}{81} \Delta \frac{2t_1-4t_2+t_3-8t_4}{\lambda U} \right]$

2. Hopping polarization

The contribution from the microscopic operator (26) can be decomposed in terms of the hopping operators

$$\begin{aligned}
 \hat{M}_u &= \frac{1}{\sqrt{2}} \mathbf{c}_i^\dagger \begin{pmatrix} 0 & 0 & 1 \\ 0 & 0 & 1 \\ -1 & -1 & 0 \end{pmatrix} \mathbf{c}_j + \text{H.c.}, \\
 \hat{M}_v &= \frac{1}{\sqrt{2}} \mathbf{c}_i^\dagger \begin{pmatrix} 0 & 0 & -1 \\ 0 & 0 & 1 \\ 1 & -1 & 0 \end{pmatrix} \mathbf{c}_j + \text{H.c.}, \text{ and} \\
 \hat{M}_w &= \mathbf{c}_i^\dagger \begin{pmatrix} 0 & 1 & 0 \\ -1 & 0 & 0 \\ 0 & 0 & 0 \end{pmatrix} \mathbf{c}_j + \text{H.c.}, \quad (47)
 \end{aligned}$$

where \hat{M}_n acts in the same representations as $(\mathbf{S}_i \times \mathbf{S}_j) \cdot \hat{\mathbf{n}}$ for $\hat{\mathbf{n}} = \hat{\mathbf{u}}, \hat{\mathbf{v}},$ and $\hat{\mathbf{w}}$. Thus, in the C_{2h} bond symmetry,

$$\mathbf{P}_{\text{hop}} = [b_1 \hat{M}_u] \hat{\mathbf{u}} + [b_2 \hat{M}_v + b_4 \hat{M}_w] \hat{\mathbf{v}} + [b_5 \hat{M}_v + b_3 \hat{M}_w] \hat{\mathbf{w}}, \quad (48)$$

and only b_4 and b_5 survive when the displacement of the ligands away from the D_{2h} symmetry is neglected. When computed in the ground state manifold of the Hamiltonian without trigonal distortion, each \hat{M}_n creates a $(\mathbf{S}_i \times \mathbf{S}_j) \cdot \hat{\mathbf{n}}$ term due to the D_{2h} symmetry. With the addition of \mathcal{H}_{CF} , using the C_{2h} character table V, we infer that the b_2 and b_4 terms mix and contribute to both \mathbb{B}_2 and \mathbb{B}_4 . Similarly the b_5 and b_3 terms mix and contribute to both \mathbb{B}_5 and \mathbb{B}_3 . Finally, the b_1 term contributes to \mathbb{B}_1 . At first order in the hopping Hamiltonian [see Eq. (24)] we have

$$\hat{M}_{n,\text{eff}} = \mathbb{P} \hat{M}_n \frac{1}{E_0 - \mathcal{H}_0} \mathcal{H}_{\text{hop}} \mathbb{P} + \text{H.c.} \quad (49)$$

Without trigonal distortion, Eq. (49) results in $\hat{M}_{n,\text{eff}} = \mathbb{M}_n (\mathbf{S}_i \times \mathbf{S}_j) \cdot \hat{\mathbf{n}}$ and thus $\mathbb{B}_4 = b_4 \mathbb{M}_w$ and $\mathbb{B}_5 = b_5 \mathbb{M}_v$. We observe that Hund's coupling is responsible for the anisotropy as $\mathbb{M}_u = \mathbb{M}_v = \mathbb{M}_w$ when $J_H/U \rightarrow 0$:

$$\lim_{J_H/U \rightarrow 0} \mathbb{M}_n = -\frac{16}{9} \frac{2t_1 + t_3}{U} \equiv \mathbb{M}. \quad (50)$$

Unlike for Eq. (44), $U \gg \lambda$ is not assumed. We see that in the limit $U \gg J_H$, the \mathbb{M}_n 's are independent of λ . The expressions for $\mathbb{M}_u, \mathbb{M}_v,$ and \mathbb{M}_w away from the $J_H/U \rightarrow 0$ limit are given in Appendix E1.

With the inclusion of the trigonal distortion at first order, we obtain additional terms. In the limiting case $U \gg J_H$,

$$\begin{aligned}
 \lim_{J_H \rightarrow 0} \hat{M}_{u,\text{eff}} &= \left[\mathbb{M} - \frac{32}{81} \Delta \frac{2t_1 + 4t_2 + t_3 + 8t_4}{\lambda U} \right] (\mathbf{S}_i \times \mathbf{S}_j)_u \\
 \lim_{J_H \rightarrow 0} \hat{M}_{v,\text{eff}} &= \left[\mathbb{M} + \frac{32}{81} \Delta \frac{2t_1 - 4t_2 + t_3 - 8t_4}{\lambda U} \right] (\mathbf{S}_i \times \mathbf{S}_j)_v \\
 &\quad + \left[\sqrt{2} \frac{32}{81} \Delta \frac{2t_1 + t_3}{\lambda U} \right] (\mathbf{S}_i \times \mathbf{S}_j)_w \\
 \lim_{J_H \rightarrow 0} \hat{M}_{w,\text{eff}} &= \left[\mathbb{M} - \frac{128}{81} \Delta \frac{t_2 + 2t_4}{\lambda U} \right] (\mathbf{S}_i \times \mathbf{S}_j)_w \\
 &\quad + \left[\sqrt{2} \frac{32}{81} \Delta \frac{2t_1 + t_3}{\lambda U} \right] (\mathbf{S}_i \times \mathbf{S}_j)_v. \quad (51)
 \end{aligned}$$

Equation (51) thus relates the coefficients b_{1-5} , obtained from the polarization integrals, to the coefficients \mathbb{B}_i at first order in \mathcal{H}_{hop} and first order in Δ . We note that the relations in Eq. (51) can be obtained without approximation numerically.

Finally, we express b_{1-5} in terms of the polarization integrals of Section V using Eq. (27). Without distortion, the ligands are in the $\hat{\mathbf{x}}$ and $\hat{\mathbf{y}}$ directions from the site i with an atomic spacing $d = a/\sqrt{2}$ so that only b_4 and b_5 are finite,

$$\begin{aligned}
 b_4 &= -P_{d\pi d\delta}^\perp - \sqrt{2} \frac{P_{pd\pi}^\parallel t_{pd\pi}}{\Delta_{pd}}, \\
 b_5 &= \frac{1}{4} \left(\sqrt{6} P_{d\sigma d\pi}^\perp - \sqrt{2} P_{d\pi d\delta}^\perp \right) + \sqrt{2} \frac{P_{p\sigma d\pi}^\perp t_{pd\pi}}{\Delta_{pd}}. \quad (52)
 \end{aligned}$$

Hence, even without the trigonal distortion, we recover the KNB formula ($b_4 = -b_5$) only when the polarization integrals are evaluated at zeroth order in d . In this case, the d - d integrals vanish and $P_{pd\pi}^\parallel = P_{p\sigma d\pi}^\perp$. The results are summarized in Table II.

In Fig. 6, we plot the coupling constants \mathbb{B}_{2-4} , calculated with exact diagonalization on a two-site cluster without any approximations, as a function of J_H , λ , and Δ in Figs. 6(a), 6(b), and 6(c), respectively. Note that we cannot decrease λ below a certain threshold in Fig. 6(b) because the pseudospin 1/2 are not well defined for $\Delta < 0$ when $\lambda = 0$ (the local ground state is fourfold degenerate). For simplicity, we assume $b_4 = -b_5$ and plotted the

constants in units of b_5 . The contributions \mathbb{B}_i cannot be compared to the contributions \mathbb{A}_i in Eq. (37) unless we accurately calculate the integrals in b_4 and b_5 , which we do not attempt here.

We see in both Figs. 5 and 6 that the KNB formula (which corresponds to $m_4 = -m_5$ and $m_{1-3} = 0$) is not accurate at all in the edge-sharing geometry, as $m_4 \neq m_5$ and all m_{1-5} are finite in any parameter range.

The expressions taking into account the displacement of the ligands towards the bond ($\phi \neq 90^\circ$) is given in Appendix A.

B. Corner-sharing geometry

In the corner-sharing geometry with $\varphi = 180^\circ$ [see Fig. 1(a)], the calculations are considerably simpler. The $\varphi \neq 180^\circ$ case is dealt with in Appendix B and is more complex due to the lack of inversion symmetry.

1. Lattice polarization

We see from Eqs. (16) and (17) that polarization along the bond vanishes. Because the only ligand is exactly at the center of the bond, its contribution also vanishes. Therefore, in contrast to the edge-sharing geometry, there is no ME coupling originating from the lattice polarization when $\varphi = 180^\circ$.

2. Hopping polarization

We define

$$\hat{N}_a = \mathbf{c}_i^\dagger \hat{\mathcal{A}}_a \mathbf{c}_j + \text{H.c.}, \quad (53)$$

in terms of the antisymmetric off-diagonal matrices $(\hat{\mathcal{A}}_a)_{bc} = \epsilon_{abc}$. Then, for an x bond, we find

$$\mathbf{P}_{\text{hop}} = \left[-t_{pd\pi} P_{p\pi d\sigma}^\perp \hat{N}_z \right] \hat{\mathbf{y}} + \left[t_{pd\pi} P_{p\pi d\sigma}^\perp \hat{N}_y \right] \hat{\mathbf{z}}, \quad (54)$$

The expressions for other types of bonds are obtained by performing the proper rotations.

Casting the above operators in the low-energy subspace with perturbation theory at first order in t and

TABLE III. Coupling coefficients defined in Eqs. (17) and (37) for the corner-sharing geometry in the $J_H/U \rightarrow 0$ limit. The CF is included through \mathcal{H}_{CF} but the displacement of the ligands is neglected

$\mathbb{A}_1 =$	0
$\mathbb{A}_2 =$	0
$\mathbb{B}_1 = -t_{pd\pi} P_{p\pi d\sigma}^\perp$	$\left[\frac{32}{9} \frac{t}{U} - \frac{64}{81} \Delta \frac{t(U+6\lambda)}{U^2\lambda} \right]$
$\mathbb{B}_2 = t_{pd\pi} P_{p\pi d\sigma}^\perp$	$\left[\frac{32}{9} \frac{t}{U} + \frac{128}{81} \Delta \frac{t(U-3\lambda)}{U^2\lambda} \right]$

Δ in the limit $U \gg J_H$, we obtain

$$\begin{aligned} \lim_{J_H/U \rightarrow 0} \hat{N}_{z,\text{eff}} &= \left[\frac{32}{9} \frac{t}{U} - \frac{64}{81} \Delta \frac{t(U+6\lambda)}{U^2\lambda} \right] (\mathbf{S}_i \times \mathbf{S}_j)_z \\ \lim_{J_H/U \rightarrow 0} \hat{N}_{y,\text{eff}} &= \left[\frac{32}{9} \frac{t}{U} + \frac{128}{81} \Delta \frac{t(U-3\lambda)}{U^2\lambda} \right] (\mathbf{S}_i \times \mathbf{S}_j)_y. \end{aligned} \quad (55)$$

As for the edge-sharing geometry, J_H is responsible for the anisotropy when $\Delta = 0$. The results are summarized in Table III. The expressions away from the $J_H/U \rightarrow 0$ limit are given in Appendix E2.

We have thus obtained an expression for the two allowed ME coupling constants of Eq. (17) as a function of the various physical parameters and integrals in the $\varphi = 180^\circ$ geometry. The deviation from the KNB formula originating from the CF thus scales Δ/λ (for large U) relatively to the KNB $\Delta = 0$ contribution. We stress that the scaling is only accurate in the $\lambda \gg \Delta$ limit.

VII. SUMMARY AND CONCLUSION

We developed a theory of the electric polarization in d^5 Mott insulators from electronic mechanisms. In particular we reconciled two approaches previously used to explain ME behaviors. On one hand, there is the ‘‘hopping polarization’’, which corresponds to formalisms principally used in the context of multiferroics, e.g. the KNB formula¹⁶ and other extensions³⁶, and relies on matrix elements such as $\langle d_{xy} | y | p_y \rangle$. With an approach similar to Slater and Koster⁴⁰, we expanded the theory by taking into account the finite distance between ions and classified the different finite polarization integrals according to their symmetry.

On the other hand, the ‘‘lattice polarization’’ is intrinsic to the Hubbard model, merely defined by the positions of the electrons on the lattice. Charge effects in single-band Mott insulators due to such effects were first discussed in Ref.²⁶ and lead to the explanation of the subgap optical conductivity in different systems on lattices with triangular loops. In a previous work, we noted that in multiorbital systems with SOC, the same mechanism was possible at second order in the hopping³⁴. In the present paper, we thoroughly considered the phenomenon and conclude that (i) in the $\Delta_{pd} \gg U$ limit, the contribution from the positions of the ligand is suppressed by a factor of U/Δ_{pd} compared to the contributions from the TM ions, which itself vanishes if the trigonal distortion $\Delta \rightarrow 0$. Both contributions are relevant in the case of α - RuCl_3 (see Fig. 5). We also conclude that (ii) the edge-sharing geometry is crucial to obtain a finite polarization operator along the TM-TM bond. In the corner-sharing geometry, even when $\varphi \neq 180^\circ$ (see Appendix B), the polarization along the bond vanishes.

The relative contributions of the two mechanisms are determined by comparing the polarization integral p_{eff} with $a \cdot t_{\text{eff}}/U$ between TM ions separated by a distance

a. Together with complementary first-principle methods to evaluate the different physical parameters, in particular the polarization integrals, the ME effects in d^5 Mott insulators can be predicted from our results. In particular, in the edge-sharing geometry the direction of the polarization changes whether $p_{\text{eff}} \ll a \cdot t_{\text{eff}}/U$, in which case \mathbb{A}_1 is finite (see Table II) and \mathbf{P} has a contribution along the bond, or $p_{\text{eff}} \gg a \cdot t_{\text{eff}}/U$, in which case \mathbf{P} is perpendicular to the bond. In any case, we generally find significant deviations from the KNB formula in the edge-sharing geometry, as can be seen in Figs. 5 and 6.

We expect that the THz optical conductivity observed in α - RuCl_3 ^{29–33} can be better understood using our results by calculating the dynamical response of the effective polarization operator in the magnetic ground state manifold, which has only been done in the pure Kitaev model³⁴.

From our results in the edge-sharing geometry of Kitaev materials, the intensities of the regular magnetic dipole-induced absorption and the electric dipole-induced absorption can be compared. Without calculating the correlation functions, the ratio of the electric dipole contribution to the magnetic dipole contribution can be estimated as $(|\hat{m}|/g\lambda)^2$, where $|\hat{m}|$ is of the order of the spin-polarization coupling constants $\{m_i\}$, g is the effective Landé g factor, and λ is the Compton wavelength³⁴. From the ‘lattice polarization’ contributions (see Table II and Fig. 5), we find that the electric dipole-induced absorption is around 20 times larger than the magnetic dipole-induced one. The ‘hopping polarization’ contribution could be even larger but cannot be estimated without calculating the integrals in Eq. (52). Finally, the electric dipole-induced absorption is expected for both in-plane and out-of-plane polarizations with similar amplitudes.

VIII. ACKNOWLEDGMENTS

A. B. thanks H. Katsura for fruitful discussions and acknowledges the Leading Graduate Course for Frontiers of Mathematical Sciences and Physics (FMSP) for the encouragement of the present paper.

Appendix A: Edge-sharing geometry with $\phi \neq 90^\circ$

Here, we consider the effect of the distortion corresponding to the two ligands moving toward the center of the bond in the $\pm\hat{\mathbf{v}}$ directions. As mentioned in Sec. III A, the displacement of the ligands is along one of the C_2 axis so that the processes will only yield coupling consistent with the D_{2h} symmetry group. This lets us study the angle dependence away from the ideal $\phi = 90^\circ$ bond geometry.

The hopping integrals can be expressed via the Slater-

Koster integrals ($t_{pd\sigma}, t_{pd\pi}, t_{dd\sigma}, t_{dd\pi}$, and $t_{dd\delta}$),

$$\begin{aligned} t_1 &= \frac{t_{dd\pi} + t_{dd\delta}}{2} + \frac{t_{pd\pi}^2}{\Delta_{pd}} \cos(\phi) \\ t_2 &= \frac{-t_{dd\pi} + t_{dd\delta}}{2} + \frac{t_{pd\pi}^2}{\Delta_{pd}} \\ t_3 &= \frac{3t_{dd\sigma} + t_{dd\delta}}{4} + \frac{3t_{pd\sigma}^2}{2\Delta_{pd}} \cos^3(\phi) \\ &\quad + \frac{(\sqrt{3}t_{pd\sigma} - t_{pd\pi})t_{pd\pi}}{\Delta_{pd}} \sin(\phi) \sin(2\phi). \end{aligned} \quad (\text{A1})$$

To be precise, we note that the integrals themselves also depend on ϕ due to the change in the TM-L distance (or alternatively in the TM-TM distance). We do not explicitly consider this dependence.⁵⁶

1. Mechanism

a. Lattice polarization

The two ligands are separated by a distance $\tilde{a} = a \cot(\phi/2)$ in the $\hat{\mathbf{v}}$ direction. The lattice polarization expression for the ligands, Eq. (45) when $\phi = 90^\circ$, becomes

$$\mathbf{P}_{\text{lat}}^{(L)} = \frac{t_{pd\pi}^2}{\Delta_{pd}^2} \sin(\phi) \left[\mathbf{c}_i^\dagger \begin{pmatrix} 0 & -1 & 0 \\ 1 & 0 & 0 \\ 0 & 0 & 0 \end{pmatrix} \mathbf{c}_j + \text{H.c.} \right] \frac{\tilde{a}}{2} \hat{\mathbf{v}}. \quad (\text{A2})$$

Here the $t_{pd\pi}$ integral also depends on ϕ if the TM-L distance $d = a/(2 \cos(\phi/2))$ varies.

b. Lattice polarization

As in the $\phi = 90^\circ$ situation, only b_4 and b_5 are nonzero without the trigonal distortion. We find,

$$\begin{aligned} b_4 &= -P_{d\pi d\delta}^\perp - 2 \sin(\phi/2) \frac{t_{pd\pi}}{\Delta_{pd}} \left(P_{pd\pi}^\parallel + \cos(\phi) (P_{pd\pi}^\parallel - P_{p\pi d\delta}^\perp) \right) \\ b_5 &= \frac{1}{4} \left(\sqrt{6} P_{d\sigma d\pi}^\perp - \sqrt{2} P_{d\pi d\delta}^\perp \right) + \frac{\sin(\phi/2)}{2} \frac{1}{\Delta_{pd}} \times \\ &\quad \left[\cos(\phi) \left(2\sqrt{3} P_{p\pi d\sigma}^\perp t_{pd\pi} + P_{p\pi d\delta}^\perp (-2\sqrt{3} t_{pd\sigma} + 6t_{pd\pi}) \right) \right. \\ &\quad \left. + \cos(2\phi) (P_{p\sigma d\pi}^\perp - P_{p\pi d\delta}^\perp) (\sqrt{3} t_{pd\sigma} - 2t_{pd\pi}) \right. \\ &\quad \left. + P_{p\sigma d\pi}^\perp (\sqrt{3} t_{pd\sigma} + 2t_{pd\pi}) + P_{p\pi d\delta}^\perp (-\sqrt{3} t_{pd\sigma} + 2t_{pd\pi}) \right]. \end{aligned} \quad (\text{A3})$$

With the addition of the trigonal distortion (displacement of the ligands perpendicular to the plane), all b_{1-5} are finite and the calculation is too cumbersome, but can be done numerically.

Appendix B: Corner-sharing geometry with $\varphi \neq 180^\circ$

In this appendix, we consider the more general corner-shared geometry where a relative rotation along the $\hat{\mathbf{z}}$ axis is allowed such that $\varphi \neq 180$ [see Fig. 1(a)]. In this case, there is no inversion symmetry at the center of the bond. The cubic orbitals are defined relatively to two sets of unit vectors $\mathcal{B}_A = \{\hat{\mathbf{x}}_A, \hat{\mathbf{y}}_A, \hat{\mathbf{z}}\}$ and $\mathcal{B}_B = \{\hat{\mathbf{x}}_B, \hat{\mathbf{y}}_B, \hat{\mathbf{z}}\}$ separated by a $2\alpha = \pi - \varphi$ rotation along the $\hat{\mathbf{z}}$ axis. We consider a uniform tetragonal distortion $\Delta_A = \Delta_B = \Delta$. A staggered tetragonal distortion (corresponding to $\Delta_A = -\Delta_B$) is also plausible, as shown in Ref.⁵⁷, but we do not consider it explicitly. For an x bond, we define $\alpha > 0$ for a displacement of the shared ligand in the $+\hat{\mathbf{y}}$ direction.

a. Full octahedral symmetry with $\alpha \neq 0$

For $\alpha \neq 0$, the symmetry group of the bond is reduced to C_{2v} . Its character table is shown in Table VII. Importantly, there is no inversion symmetry at the center of the bond. Thus, the hopping can be antisymmetric and the polarization can couple to symmetric two-spin operators. The full ME coupling is then characterized by at most thirty coefficients instead of nine.

The effective hopping matrices between the t_{2g} orbitals of site i and j are

$$\hat{T}_x(C_{2v}) = \begin{pmatrix} t_1 & t_4 & 0 \\ -t_4 & t_2 & 0 \\ 0 & 0 & t_3 \end{pmatrix} \quad \text{and} \quad \hat{T}_y(C_{2v}) = \begin{pmatrix} t_2 & t_4 & 0 \\ -t_4 & t_1 & 0 \\ 0 & 0 & t_3 \end{pmatrix}. \quad (\text{B1})$$

Considering only indirect p - d hopping and working in the \mathcal{B}_A and \mathcal{B}_B bases, we have simply

$$\hat{T}_x = \begin{pmatrix} 0 & 0 & 0 \\ 0 & t_2 & 0 \\ 0 & 0 & t_2 \cos(2\alpha) \end{pmatrix}_{\mathcal{B}_A, \mathcal{B}_B} \quad \text{and} \quad (\text{B2})$$

$$\hat{T}_y = \begin{pmatrix} t_2 & 0 & 0 \\ 0 & 0 & 0 \\ 0 & 0 & t_2 \cos(2\alpha) \end{pmatrix}_{\mathcal{B}_A, \mathcal{B}_B}. \quad (\text{B3})$$

The ME coupling (for an x bond) becomes

$$\begin{aligned} \mathbf{P} &= \begin{pmatrix} 0 & 0 & 0 \\ 0 & 0 & m_1^A \\ 0 & m_2^A & 0 \end{pmatrix} (\mathbf{S}_i \times \mathbf{S}_j) \\ &+ \begin{pmatrix} 0 & 0 & 0 & 0 \\ m_0^D & m_1^D & m_2^D & m_3^D \\ 0 & 0 & 0 & 0 \end{pmatrix} \begin{pmatrix} \mathbb{I} \\ S_i^x S_j^x \\ S_i^y S_j^y \\ S_i^z S_j^z \end{pmatrix} \\ &+ \begin{pmatrix} 0 & 0 & m_1^\Gamma \\ 0 & 0 & 0 \\ m_2^\Gamma & 0 & 0 \end{pmatrix} \begin{pmatrix} S_i^y S_j^z + S_i^z S_j^y \\ S_i^x S_j^z + S_i^z S_j^x \\ S_i^x S_j^y + S_i^y S_j^x \end{pmatrix}. \quad (\text{B4}) \end{aligned}$$

Spin operators in the $\mathcal{B}_{A(B)}$ basis are obtained by the transformation $\mathbf{S}_i \rightarrow e^{i\alpha S^z} \mathbf{S}_i e^{-i\alpha S^z}$ ($\mathbf{S}_j \rightarrow e^{-i\alpha S^z} \mathbf{S}_j e^{i\alpha S^z}$). When considering the two-spin operators, the change of basis $(\mathcal{B}, \mathcal{B}) \rightarrow (\mathcal{B}_A, \mathcal{B}_B)$ does not change the representation of the operators, so that Eq. (B4) is valid with spin operators written in either set of bases (the values of the coefficients are nevertheless modified). From now on we work with the \mathcal{B} basis for \mathbf{P} and in the \mathcal{B}_A and \mathcal{B}_B bases for \mathbf{S}_i and \mathbf{S}_j , respectively.

b. Tetragonal distortion

For a uniform tetragonal distortion, the C_{2v} symmetry group is not affected by Δ and the form of \hat{m} does not change.

1. Mechanism

a. Lattice polarization

We see from Eq. (B4) that polarization along the bond is only possible via m_1^Γ . However, as discussed in Sec. VIA, the contribution from the TM ions must vanish when the hopping is diagonal with respect to the pseudospins, which happens when the 3×3 matrices defining the tetragonal CF and the hopping commute. In the present case, due to the forms of \mathcal{H}_{CF} and (B1), both matrices always commute even in the lowest symmetry, so that $\mathbf{P}_{\text{lat}}^{(\text{TM})} = 0$.

The ligand contribution corresponds exactly to the hopping matrix (neglecting d - d direct hopping),

$$\mathbf{P}_{\text{lat},x}^{(\text{L})} = \tan(\alpha) \left[\mathbf{c}_i^\dagger \hat{T}_x \mathbf{c}_j + \text{H.c.} \right] \frac{a}{2} \hat{\mathbf{y}} \quad (\text{B5})$$

$$\mathbf{P}_{\text{lat},y}^{(\text{L})} = -\tan(\alpha) \left[\mathbf{c}_i^\dagger \hat{T}_y \mathbf{c}_j + \text{H.c.} \right] \frac{a}{2} \hat{\mathbf{x}}. \quad (\text{B6})$$

We show in the next subsection that such microscopic operators will, in turn, only produce a coupling with diagonal two-spin operators $S_i^\alpha S_j^\alpha$ in addition to a spin-independent polarization (expected due to the lack of inversion symmetry).

b. Hopping polarization

For an x bond, we find

$$\mathbf{P}_{\text{hop}} = \left[\hat{N}_S^x + \hat{N}_A^x \right] \hat{\mathbf{x}} + \left[\hat{N}_S^y + \hat{N}_A^y \right] \hat{\mathbf{y}} + \left[\hat{N}_S^z + \hat{N}_A^z \right] \hat{\mathbf{z}}, \quad (\text{B7})$$

with

$$\hat{N}_{S/A}^a = \mathbf{c}_i^\dagger \hat{N}_{S/A}^a \mathbf{c}_j + \text{H.c.}, \quad (\text{B8})$$

where S and A stand for symmetric and antisymmetric, which are both allowed when $\alpha \neq 0$ due to the lack of

inversion symmetry at the center of the bonds. Denoting the antisymmetric and symmetric off-diagonal matrices by $(\hat{A}_a)_{bc} = \epsilon_{abc}$ and $(\hat{S}_a)_{bc} = |\epsilon_{abc}|$, respectively (ϵ is the Levi-Civita tensor), we have

$$\begin{aligned} \hat{N}_S^x &= \sin(\alpha) t_{pd\pi} P_{p\pi d\sigma}^\perp \hat{S}_z, & \hat{N}_A^x &= 0, \\ \hat{N}_S^y &= -2 \sin(\alpha) t_{pd\pi} \times \\ & \left(\begin{array}{cc} 0 & 0 \\ 0 & P_{pd\pi}^\parallel & 0 \\ 0 & 0 & P_{p\sigma d\pi}^\perp + (P_{pd\pi}^\parallel + P_{p\sigma d\pi}^\perp) \cos(2\alpha) \end{array} \right), \\ \hat{N}_A^y &= -\cos(\alpha) t_{pd\pi} P_{p\pi d\sigma}^\perp \hat{A}_z, \\ \hat{N}_S^z &= -\sin(2\alpha) t_{pd\pi} P_{p\sigma d\pi}^\perp \hat{S}_x, \\ \hat{N}_A^z &= \cos(2\alpha) t_{pd\pi} P_{p\pi d\sigma}^\perp \hat{A}_y. \end{aligned} \quad (\text{B9})$$

The expressions for a y bond are obtained by performing a $\pi/2$ rotation around $\hat{\mathbf{z}}$.

Casting the above operators in the low-energy subspace, we obtained the effective polarization operator. First, even in the C_{2v} , we can read from the character tables that $\hat{A}_{a,\text{eff}} = \mathbf{a}_a (\mathbf{S}_i \times \mathbf{S}_j)_a$ and $\hat{S}_{a,\text{eff}} = \mathfrak{s}_a |\epsilon_{abc}| S_i^b S_j^c$, respectively. For the antisymmetric part, the results from perturbation theory in the limit $U \gg J_H$ are

$$\begin{aligned} \mathbf{a}_z &= \frac{32 t_2 \cos^2(\alpha)}{9 U} + \Delta \frac{64 t_2 (-2U - 3\lambda + (U - 3\lambda) \cos(2\alpha))}{81 U^2 \lambda} \\ \mathbf{a}_y &= \frac{32 t_2 \cos^2(\alpha)}{9 U} + \Delta \frac{32 t_2 (-U - 6\lambda + (5U - 6\lambda) \cos(2\alpha))}{81 U^2 \lambda}. \end{aligned} \quad (\text{B10})$$

As for the edge-sharing geometry, we observe that J_H is responsible for the anisotropy when $\Delta = 0$. For the symmetric part, the off-diagonal matrices give a contribution that is proportional to J_H . In the $U \gg J_H$ limit,

$$\begin{aligned} \mathfrak{s}_z &= \frac{32 t_2 J_H (1 - 2 \cos(2\alpha))}{9 (2U + 3\lambda)^2} \\ & - \Delta \frac{128 t_2 J_H (2U - 9\lambda) (-1 + 2 \cos(2\alpha))}{81 \lambda (2U + 3\lambda)^2} \\ \mathfrak{s}_x &= \frac{64 t_2 J_H \cos^2(\alpha)}{9 (2U + 3\lambda)^2} \\ & - \Delta \frac{128 t_2 J_H (U + 18\lambda + (U + 9\lambda) \cos(2\alpha))}{81 \lambda (2U + 3\lambda)^2}. \end{aligned} \quad (\text{B11})$$

Finally, the diagonal terms in Eq. (B9) each give a constant and three $S_i^a S_j^a$ terms with $a = x, y$, and z . Moreover, in the absence of J_H , the contribution is isotropic.

In the $U \gg J_H$ and $U \gg \lambda$ limit,

$$\begin{aligned} \begin{pmatrix} 0 & 0 & 0 \\ 0 & 1 & 0 \\ 0 & 0 & 0 \end{pmatrix} &\rightarrow \left[\frac{16 t_2 \cos^2(\alpha)}{9 U} + \Delta \frac{32 t_2 (-2 + \cos(2\alpha))}{81 \lambda U} \right] \mathbf{S}_i \cdot \mathbf{S}_j \\ &+ \frac{8 t_2 (-5 + \cos(2\alpha))}{9 U} + \Delta \frac{32 t_2 (4 + \cos(2\alpha))}{81 \lambda U}, \\ \begin{pmatrix} 0 & 0 & 0 \\ 0 & 0 & 0 \\ 0 & 0 & 1 \end{pmatrix} &\rightarrow \left[\frac{16 t_2 \cos^2(\alpha)}{9 U} + \Delta \frac{32 t_2 (1 + 4 \cos(2\alpha))}{81 \lambda U} \right] \mathbf{S}_i \cdot \mathbf{S}_j \\ &+ \frac{8 t_2 (1 - 5 \cos(2\alpha))}{9 U} + \Delta \frac{32 t_2 (1 - 8 \cos(2\alpha))}{81 \lambda U}. \end{aligned} \quad (\text{B12})$$

We have thus obtained an expression for all the ME coupling constants of Eq. (B4) as a function of the various physical parameters and integrals.

Appendix C: Character tables

Here we show the character tables **IV** to **VII** and the different functions corresponding to each irreducible representations for the symmetry groups mentioned throughout the paper.

TABLE IV. Character table of D_{2h} with twofold axis in the a , b , and c directions. $C_{2,\alpha}$ is a C_2 rotation along the corresponding axis ($\alpha = a, b$, or c), $\sigma_{\alpha\beta}$ is a reflection across the $\alpha\beta$ plane, and the $\langle ij \rangle$ bond is in the a direction.

D_{2h}	E	$C_{2,a}$	$C_{2,b}$	$C_{2,c}$	I	σ_{bc}	σ_{ac}	σ_{ab}	functions
A_g	1	1	1	1	1	1	1	1	-
$B_{1,g}$	1	1	-1	-1	1	1	-1	-1	S^a
$B_{2,g}$	1	-1	1	-1	1	-1	1	-1	S^b
$B_{3,g}$	1	-1	-1	1	1	-1	-1	1	S^c
A_u	1	1	1	1	-1	-1	-1	-1	$(\mathbf{S}_i \times \mathbf{S}_j)_a$
$B_{1,u}$	1	1	-1	-1	-1	-1	1	1	a , i - j antisym.
$B_{2,u}$	1	-1	1	-1	-1	1	-1	1	b , $(\mathbf{S}_i \times \mathbf{S}_j)_b$
$B_{3,u}$	1	-1	-1	1	-1	1	1	-1	c , $(\mathbf{S}_i \times \mathbf{S}_j)_c$

TABLE V. Character table of C_{2h} with twofold axis in the a direction. $C_{2,a}$ is the C_2 rotation around $\hat{\mathbf{a}}$, σ_{bc} is the reflection across the plane perpendicular to $\hat{\mathbf{a}}$, and the $\langle ij \rangle$ bond is along the a direction.

C_{2h}	E	$C_{2,a}$	I	σ_{bc}	functions
A_g	1	1	1	1	S^a
B_g	1	-1	1	-1	S^b, S^c
A_u	1	1	-1	-1	a , $(\mathbf{S}_i \times \mathbf{S}_j)_a$, i - j antisym.
B_u	1	-1	-1	1	b , $(\mathbf{S}_i \times \mathbf{S}_j)_b$ c , $(\mathbf{S}_i \times \mathbf{S}_j)_c$

TABLE VI. Character table of D_{4h} with $\hat{\mathbf{a}}$ as the C_4 axis. The $2C_2'$ rotations are around $\hat{\mathbf{b}}$ and $\hat{\mathbf{c}}$, the $2C_2''$ ones around $\hat{\mathbf{b}} \pm \hat{\mathbf{c}}$, and $2\sigma_{v,d}$ are the corresponding reflections. The $\langle ij \rangle$ bond is along $\hat{\mathbf{a}}$.

D_{4h}	E	$2C_{4,a}$	$C_{2,a}$	$2C_2'$	$2C_2''$	I	$2S_4$	σ_{bc}	$2\sigma_v$	$2\sigma_d$	functions
$A_{1,g}$	1	1	1	1	1	1	1	1	1	1	-
$A_{2,g}$	1	1	1	-1	-1	1	1	1	-1	-1	S^a
$B_{1,g}$	1	-1	1	1	-1	1	-1	1	1	-1	-
$B_{2,g}$	1	-1	1	-1	1	1	-1	1	-1	1	bc
E_g	2	0	-2	0	0	2	0	-2	0	0	(S^b, S^c) , (ac, ab)
$A_{1,u}$	1	1	1	1	1	-1	-1	-1	-1	-1	-
$A_{2,u}$	1	1	1	-1	-1	-1	-1	-1	1	1	a , i - j antisym.
$B_{1,u}$	1	-1	1	1	-1	-1	1	-1	-1	1	$(\mathbf{S}_i \times \mathbf{S}_j)_a$
$B_{2,u}$	1	-1	1	-1	1	-1	1	-1	1	-1	-
E_u	2	0	-2	0	0	-2	0	2	0	0	(b, c) , $((\mathbf{S}_i \times \mathbf{S}_j)_b, (\mathbf{S}_i \times \mathbf{S}_j)_c)$

TABLE VII. Character table of C_{2v} . The $\langle ij \rangle$ bond is along the $\hat{\mathbf{x}}$ axis.

C_{2v}	E	$C_{2,y}$	σ_{xy}	σ_{yz}	functions
A_1	1	1	1	1	y , $(\mathbf{S}_i \times \mathbf{S}_j)_z$
A_2	1	1	-1	-1	xz , S^y , $(\mathbf{S}_i \times \mathbf{S}_j)_x$
B_1	1	-1	1	-1	x , xy , S^y , i - j antisym.
B_2	1	-1	-1	1	z , yz , S^y , $(\mathbf{S}_i \times \mathbf{S}_j)_y$

Appendix D: Polarization integrals

In Table VIII we list the polarization integrals for a general bond direction in a manner similar to that of Ref.⁴⁰. The entries not given can be found by cyclically permuting the coordinates and direction cosines.

TABLE VIII. Polarization integrals in terms of two-center integrals for two ions separated by a vector $\mathbf{d} = \|\mathbf{d}\|(l, m, n)$. Only the p - t_{2g} and t_{2g} - t_{2g} integrals are considered.

$\langle p_x x d_{yz}\rangle =$	$\sqrt{3}l^2mnP_{pd\sigma}^{\parallel} - 2l^2mnP_{pd\pi}^{\parallel} + \sqrt{3}mn(1-l^2)P_{p\pi d\sigma}^{\perp} - 2l^2mnP_{p\sigma d\pi}^{\perp} + mn(1+l^2)P_{p\pi d\delta}^{\perp}$
$\langle p_x y d_{yz}\rangle =$	$\sqrt{3}lm^2nP_{pd\sigma}^{\parallel} - 2lm^2nP_{pd\pi}^{\parallel} - \sqrt{3}lm^2nP_{p\pi d\sigma}^{\perp} + ln(1-2m^2)P_{p\sigma d\pi}^{\perp} - ln(1-m^2)P_{p\pi d\delta}^{\perp}$
$\langle p_x z d_{xy}\rangle =$	$\sqrt{3}lmn^2P_{pd\sigma}^{\parallel} - 2lmn^2P_{pd\pi}^{\parallel} - \sqrt{3}lmn^2P_{p\pi d\sigma}^{\perp} + lm(1-2n^2)P_{p\sigma d\pi}^{\perp} - lm(1-n^2)P_{p\pi d\delta}^{\perp}$
$\langle p_x x d_{xz}\rangle =$	$\sqrt{3}l^3nP_{pd\sigma}^{\parallel} + ln(1-2l^2)P_{pd\pi}^{\parallel} + \sqrt{3}ln(1-l^2)P_{p\pi d\sigma}^{\perp} + ln(1-2l^2)P_{p\sigma d\pi}^{\perp} - ln(1-l^2)P_{p\pi d\delta}^{\perp}$
$\langle p_x y d_{xz}\rangle =$	$\sqrt{3}l^2mnP_{pd\sigma}^{\parallel} + mn(1-2l^2)P_{pd\pi}^{\parallel} - \sqrt{3}l^2mnP_{p\pi d\sigma}^{\perp} - 2l^2mnP_{p\sigma d\pi}^{\perp} - mn(1-l^2)P_{p\pi d\delta}^{\perp}$
$\langle p_x z d_{xz}\rangle =$	$\sqrt{3}l^2n^2P_{pd\sigma}^{\parallel} + n^2(1-2l^2)P_{pd\pi}^{\parallel} - \sqrt{3}l^2n^2P_{p\pi d\sigma}^{\perp} + l^2(1-2n^2)P_{p\sigma d\pi}^{\perp} + (1-l^2)(1-n^2)P_{p\pi d\delta}^{\perp}$
$\langle p_x x d_{xy}\rangle =$	$\sqrt{3}l^3mP_{pd\sigma}^{\parallel} + lm(1-2l^2)P_{pd\pi}^{\parallel} + \sqrt{3}lm(1-l^2)P_{p\pi d\sigma}^{\perp} + lm(1-2l^2)P_{p\sigma d\pi}^{\perp} - lm(1-l^2)P_{p\pi d\delta}^{\perp}$
$\langle p_x y d_{xy}\rangle =$	$\sqrt{3}l^2m^2P_{pd\sigma}^{\parallel} + m^2(1-2l^2)P_{pd\pi}^{\parallel} - \sqrt{3}l^2m^2P_{p\pi d\sigma}^{\perp} + l^2(1-2m^2)P_{p\sigma d\pi}^{\perp} + (1-l^2)(1-m^2)P_{p\pi d\delta}^{\perp}$
$\langle p_x z d_{xy}\rangle =$	$\sqrt{3}l^2mnP_{pd\sigma}^{\parallel} + mn(1-2l^2)P_{pd\pi}^{\parallel} - \sqrt{3}l^2mnP_{p\pi d\sigma}^{\perp} - l^2mnP_{p\sigma d\pi}^{\perp} - mn(1-l^2)P_{p\pi d\delta}^{\perp}$
$\langle d_{yz} x d_{yz}\rangle =$	0
$\langle d_{yz} y d_{yz}\rangle =$	0
$\langle d_{yz} z d_{yz}\rangle =$	0
$\langle d_{yz} x d_{xz}\rangle =$	$\sqrt{3}mn^2P_{d\sigma d\pi}^{\perp} + m(1-3n^2)P_{d\pi d\delta}^{\perp}$
$\langle d_{yz} y d_{xz}\rangle =$	$-\sqrt{3}ln^2P_{d\sigma d\pi}^{\perp} - l(1-3n^2)P_{d\pi d\delta}^{\perp}$
$\langle d_{yz} z d_{xz}\rangle =$	0
$\langle d_{yz} x d_{xy}\rangle =$	$\sqrt{3}m^2nP_{d\sigma d\pi}^{\perp} + n(1-3m^2)P_{d\pi d\delta}^{\perp}$
$\langle d_{yz} y d_{xy}\rangle =$	0
$\langle d_{yz} z d_{xy}\rangle =$	$-\sqrt{3}lm^2P_{d\sigma d\pi}^{\perp} - l(1-3m^2)P_{d\pi d\delta}^{\perp}$

Appendix E: Full expressions of the coupling constants

Here we give the full expressions calculated with perturbation theory of the coupling constants \mathbb{A}_i and \mathbb{B}_i calculated in Sec. VI. The expressions are thus exact in U , λ , and J_H in the limit of vanishing Δ .

1. Edge-sharing geometry

Except for \mathbb{A}_1 , the nonvanishing coupling constants (\mathbb{A}_2 , \mathbb{A}_4 , \mathbb{B}_{2-5}) can be found from the operators \hat{M}_u , \hat{M}_v , and \hat{M}_w defined in Eq. (47). In the following, we give the explicit expression of \mathbb{A}_1 obtained from Eq. (42) (linear in Δ), and the expressions for \hat{M}_u , \hat{M}_v , and \hat{M}_w

calculated with Eq. (49) (here we only explicitly give the expressions without trigonal distortion, i.e., $\Delta = 0$ and $t_4 = 0$). As mentioned in Eq. (43),

$$\mathbb{A}_1 = \sqrt{2}\frac{64}{81}\Delta(t_1 + t_2 - t_3 - t_4)\frac{J_H}{\lambda} \times \frac{P}{Q}. \quad (\text{E1})$$

Without trigonal distortion, from Eq. (49) we find $\hat{M}_{n,\text{eff}} = \mathbb{M}_n(\mathbf{S}_i \times \mathbf{S}_j) \cdot \hat{\mathbf{n}}$ with

$$\mathbb{M}_n = -\frac{16}{9}\frac{R_n}{S}, \quad (\text{E2})$$

where $n = u, v, w$ (and $\hat{\mathbf{n}} = \hat{\mathbf{u}}, \hat{\mathbf{v}},$ and $\hat{\mathbf{w}}$, respectively).

The polynomials P , Q , $R_{u,v,w}$, and S are given by

$$\begin{aligned}
P = & 2(3\lambda + U)^5(3\lambda + 2U) \left(8U^3(t_1 + t_2 + t_3) + 3\lambda U^2(11t_1 + 7t_2 + 9t_3) + 9\lambda^3(2t_1 + t_3) + 24\lambda^2 U(2t_1 + t_3) \right) \\
& - J_H(3\lambda + U)^2 \left(448U^6(t_1 + t_2 + t_3) + 112\lambda U^5(53t_1 + 45t_2 + 49t_3) + 2\lambda^2 U^4(15659t_1 + 10719t_2 + 13189t_3) \right. \\
& \quad + 18\lambda^3 U^3(4717t_1 + 2333t_2 + 3525t_3) + 72\lambda^4 U^2(1732t_1 + 498t_2 + 1115t_3) \\
& \quad \left. + 27\lambda^5 U(3446t_1 + 336t_2 + 1891t_3) + 13365\lambda^6(2t_1 + t_3) \right) \\
& + 3J_H^2(3\lambda + U) \left(9\lambda^6(10474t_1 + 672t_2 + 5573t_3) + 736U^6(t_1 + t_2 + t_3) + 4\lambda U^5(2923t_1 + 2271t_2 + 2597t_3) \right. \\
& \quad + 8\lambda^2 U^4(8882t_1 + 5412t_2 + 7147t_3) + 10\lambda^3 U^3(21673t_1 + 9893t_2 + 15783t_3) \\
& \quad \left. + 2\lambda^4 U^2(176705t_1 + 54033t_2 + 115369t_3) + 15\lambda^5 U(19466t_1 + 3192t_2 + 11329t_3) \right) \\
& - J_H^3 \left(27\lambda^6(54166t_1 + 4640t_2 + 29403t_3) + 3008U^6(t_1 + t_2 + t_3) + 48\lambda U^5(1663t_1 + 835t_2 + 1249t_3) \right. \\
& \quad + 300\lambda^2 U^4(2109t_1 + 697t_2 + 1403t_3) + 2\lambda^3 U^3(1156429t_1 + 268369t_2 + 712399t_3) \\
& \quad \left. + 6\lambda^4 U^2(723347t_1 + 116579t_2 + 419963t_3) + 9\lambda^5 U(449042t_1 + 48856t_2 + 248949t_3) \right) \\
& - J_H^4 \left(-17\lambda^5(71174t_1 - 9816t_2 + 30679t_3) + 10784U^5(t_1 + t_2 + t_3) + 20\lambda U^4(353t_1 + 6237t_2 + 3295t_3) \right. \\
& \quad + 10\lambda^2 U^3(-41005t_1 + 54207t_2 + 6601t_3) - 4\lambda^3 U^2(423514t_1 - 268196t_2 + 77659t_3) \\
& \quad \left. - 14\lambda^4 U(176362t_1 - 63564t_2 + 56399t_3) \right) \\
& - 6J_H^5 \left(2\lambda^4(22394t_1 - 45660t_2 - 11633t_3) - 6944U^4(t_1 + t_2 + t_3) - 8\lambda U^3(4555t_1 + 8163t_2 + 6359t_3) \right. \\
& \quad \left. - 3\lambda^2 U^2(14845t_1 + 70569t_2 + 42707t_3) + 2\lambda^3 U(12386t_1 - 132544t_2 - 60079t_3) \right) \\
& - 36J_H^6 \left(4\lambda^3(1238t_1 + 560t_2 + 899t_3) + 776U^3(t_1 + t_2 + t_3) + 3\lambda U^2(1511t_1 + 1707t_2 + 1609t_3) \right. \\
& \quad \left. + 6\lambda^2 U(1342t_1 + 1560t_2 + 1451t_3) \right) \\
& - 216J_H^7 \left(\lambda^2(233t_1 + 2637t_2 + 1435t_3) + 344U^2(t_1 + t_2 + t_3) + 2\lambda U(395t_1 + 999t_2 + 697t_3) \right) \\
& - 1296J_H^8 (-\lambda(137t_1 + 315t_2 + 226t_3) - 104U + (t_1 + t_2 + t_3)) \\
& - 62208J_H^9(t_1 + t_2 + t_3), \tag{E3}
\end{aligned}$$

$$Q = (6J_H - 3\lambda - 2U)^2 (6J_H^2 + J_H(4\lambda + U) - U(3\lambda + U))^2 (6J_H^2 - J_H(17\lambda + 8U) + (3\lambda + U)(3\lambda + 2U))^3 \tag{E4}$$

$$\begin{aligned}
R_u = & (2t_1 + t_3)(3\lambda + U)^2(3\lambda + 2U)^2 \\
& - 2J_H(3\lambda + U) (2U^2(13t_1 + t_2 + 7t_3) + 2\lambda U(53t_1 + 3t_2 + 28t_3) + 51\lambda^2(2t_1 + t_3)) \\
& + J_H^2 (\lambda^2(634t_1 + 48t_2 + 341t_3) + 8U^2(12t_1 + 2t_2 + 7t_3) + 4\lambda U(126t_1 + 16t_2 + 71t_3)) \\
& - 12J_H^3(\lambda(12t_1 - 2t_2 + 5t_3) + U(3t_1 - t_2 + t_3)) \\
& - 36J_H^4(2t_2 + t_3), \tag{E5}
\end{aligned}$$

$$\begin{aligned}
R_v = & (2t_1 + t_3)(3\lambda + U)^2(3\lambda + 2U)^2 \\
& - 2J_H(3\lambda + U) (2U^2(13t_1 - t_2 + 7t_3) + 2\lambda U(53t_1 - 3t_2 + 28t_3) + 51\lambda^2(2t_1 + t_3)) \\
& + J_H^2 (\lambda^2(634t_1 - 48t_2 + 341t_3) + 8U^2(12t_1 - 2t_2 + 7t_3) + 4\lambda U(126t_1 - 16t_2 + 71t_3)) \\
& - 12J_H^3(\lambda(12t_1 + 2t_2 + 5t_3) + U(3t_1 + t_2 + t_3)) \\
& - 36J_H^4(t_3 - 2t_2), \tag{E6}
\end{aligned}$$

$$\begin{aligned}
R_w = & (2t_1 + t_3)(3\lambda + U)^2(3\lambda + 2U)^2 \\
& - 2J_H(3\lambda + U) (51\lambda^2(2t_1 + t_3) + 4U^2(7t_1 + 3t_3) + 2\lambda U(56t_1 + 25t_3)) \\
& + J_H^2 (\lambda^2(682t_1 + 293t_3) + 8U^2(14t_1 + 5t_3) + 4\lambda U(142t_1 + 55t_3)) \\
& - 12J_H^3(\lambda(10t_1 + 7t_3) + 2U(t_1 + t_3)) \\
& - 36J_H^4(2t_1 - t_3), \tag{E7}
\end{aligned}$$

$$S = (6J_H - 3\lambda - 2U) (6J_H^2 + J_H(4\lambda + U) - U(3\lambda + U)) (6J_H^2 - J_H(17\lambda + 8U) + (3\lambda + U)(3\lambda + 2U)). \tag{E8}$$

2. Corner-sharing geometry

In the corner-sharing geometry, $\mathbb{A}_1 = \mathbb{A}_2 = 0$, and only the hopping polarization is nontrivial. It is calculated from the hopping operators \hat{N}_y and \hat{N}_z defined in Eq. (53). Without tetragonal distortion ($\Delta = 0$), using Eq. (49) we find $\hat{N}_{y,\text{eff}} = \mathbb{N}(\mathbf{S}_i \times \mathbf{S}_j) \cdot \hat{\mathbf{y}}$ and $\hat{N}_{z,\text{eff}} = \mathbb{N}(\mathbf{S}_i \times \mathbf{S}_j) \cdot \hat{\mathbf{z}}$, with $\mathbb{N} = \frac{32}{9} \times \frac{P'}{Q'}$ and

$$\begin{aligned}
P' = & (9\lambda^2 + 2U^2 + 9\lambda U)^2 \\
& - 2J_H(3\lambda + U) (51\lambda^2 + 13U^2 + 53\lambda U) \\
& + J_H^2 (317\lambda^2 + 48U^2 + 252\lambda U) \\
& - 18J_H^3(4\lambda + U), \tag{E9}
\end{aligned}$$

$$\begin{aligned}
Q' = & (6J_H - 3\lambda - 2U) (6J_H^2 + J_H(4\lambda + U) - U(3\lambda + U)) \\
& \times (6J_H^2 - J_H(17\lambda + 8U) + (3\lambda + U)(3\lambda + 2U)). \tag{E10}
\end{aligned}$$

REFERENCES

- * bolens@spin.phys.s.u-tokyo.ac.jp
- ¹ T. Kimura, T. Goto, H. Shintani, K. Ishizaka, T.-h. Arima, and Y. Tokura, *Nature* **426**, 55 (2003).
 - ² J. Wang, J. Neaton, H. Zheng, V. Nagarajan, S. Ogale, B. Liu, D. Viehland, V. Vaithyanathan, D. Schlom, U. Waghmare, *et al.*, *Science* **299**, 1719 (2003).
 - ³ N. Hur, S. Park, P. Sharma, J. Ahn, S. Guha, and S. Cheong, *Nature* **429**, 392 (2004).
 - ⁴ M. Fiebig, *Journal of Physics D: Applied Physics* **38**, R123 (2005).
 - ⁵ W. Eerenstein, N. Mathur, and J. F. Scott, *Nature* **442**, 759 (2006).
 - ⁶ S.-W. Cheong and M. Mostovoy, *Nature materials* **6**, 13 (2007).
 - ⁷ Y. Tokura, S. Seki, and N. Nagaosa, *Rep. Prog. Phys.* **77**, 076501 (2014).
 - ⁸ A. Pimenov, A. Mukhin, V. Y. Ivanov, V. Travkin, A. Balbashov, and A. Loidl, *Nature Physics* **2**, 97 (2006).
 - ⁹ A. Sushkov, R. V. Aguilar, S. Park, S. Cheong, and H. Drew, *Phys. Rev. Lett.* **98**, 027202 (2007).
 - ¹⁰ H. Katsura, A. V. Balatsky, and N. Nagaosa, *Phys. Rev. Lett.* **98**, 027203 (2007).
 - ¹¹ M. Cazayous, Y. Gallais, A. Sacuto, R. de Sousa, D. Lebeugle, and D. Colson, *Phys. Rev. Lett.* **101**, 037601 (2008).
 - ¹² S. Seki, N. Kida, S. Kumakura, R. Shimano, and Y. Tokura, *Phys. Rev. Lett.* **105**, 097207 (2010).
 - ¹³ Y. Takahashi, R. Shimano, Y. Kaneko, H. Murakawa, and Y. Tokura, *Nature Physics* **8**, 121 (2012).
 - ¹⁴ S. H. Chun, K. W. Shin, H. J. Kim, S. Jung, J. Park, Y.-M. Bahk, H.-R. Park, J. Kyoung, D.-H. Choi, D.-S. Kim, *et al.*, *Phys. Rev. Lett.* **120**, 027202 (2018).
 - ¹⁵ I. A. Sergienko, C. Şen, and E. Dagotto, *Phys. Rev. Lett.* **97**, 227204 (2006).
 - ¹⁶ H. Katsura, N. Nagaosa, and A. V. Balatsky, *Phys. Rev. Lett.* **95**, 057205 (2005).
 - ¹⁷ M. Mostovoy, *Phys. Rev. Lett.* **96**, 067601 (2006).
 - ¹⁸ I. A. Sergienko and E. Dagotto, *Phys. Rev. B* **73**, 094434 (2006).
 - ¹⁹ C. Jia, S. Onoda, N. Nagaosa, and J. H. Han, *Phys. Rev. B* **74**, 224444 (2006).
 - ²⁰ C. Jia, S. Onoda, N. Nagaosa, and J. H. Han, *Phys. Rev. B* **76**, 144424 (2007).
 - ²¹ T.-h. Arima, *J. Phys. Soc. Jpn.* **76**, 073702 (2007).
 - ²² T.-K. Ng and P. A. Lee, *Phys. Rev. Lett.* **99**, 156402 (2007).
 - ²³ A. C. Potter, T. Senthil, and P. A. Lee, *Phys. Rev. B* **87**, 245106 (2013).
 - ²⁴ S. Elsässer, D. Wu, M. Dressel, and J. A. Schlueter, *Phys. Rev. B* **86**, 155150 (2012).
 - ²⁵ D. V. Pilon, C. H. Lui, T.-H. Han, D. Shrekenhamer, A. J. Frenzel, W. J. Padilla, Y. S. Lee, and N. Gedik, *Phys. Rev. Lett.* **111**, 127401 (2013).
 - ²⁶ L. N. Bulaevskii, C. D. Batista, M. V. Mostovoy, and D. I. Khomskii, *Phys. Rev. B* **78**, 024402 (2008).
 - ²⁷ Y. Huh, M. Punk, and S. Sachdev, *Phys. Rev. B* **87**, 235108 (2013).
 - ²⁸ K. Hwang, S. Bhattacharjee, and Y. B. Kim, *New J. Phys* **16**, 123009 (2014).
 - ²⁹ A. Little, L. Wu, P. Lampen-Kelley, A. Banerjee, S. Patankar, D. Rees, C. A. Bridges, J.-Q. Yan, D. Mandrus, S. E. Nagler, and J. Orenstein, *Phys. Rev. Lett.* **119**, 227201 (2017).
 - ³⁰ Z. Wang, S. Reschke, D. Hivonen, S.-H. Do, K.-Y. Choi, M. Gensch, U. Nagel, T. Rößm, and A. Loidl, *Phys. Rev. Lett.* **119**, 227202 (2017).
 - ³¹ C. Wellm, J. Zeisner, A. Alfonsov, A. Wolter, M. Roslova, A. Isaeva, T. Doert, M. Vojta, B. Büchner, and V. Kataev, *arXiv:1710.00670* (2017).
 - ³² S. Reschke, F. Mayr, S. Widmann, H.-A. K. von Nidda, V. Tsurkan, M. Eremin, S.-H. Do, K.-Y. Choi, Z. Wang, and A. Loidl, *arXiv:1803.04887* (2018).
 - ³³ L. Shi, Y. Liu, T. Lin, M. Zhang, S. Zhang, L. Wang, Y. Shi, T. Dong, and N. Wang, *arXiv:1803.08398* (2018).
 - ³⁴ A. Bolens, H. Katsura, M. Ogata, and S. Miyashita, *Phys. Rev. B* **97**, 161108 (2018).
 - ³⁵ T. A. Kaplan and S. D. Mahanti, *Phys. Rev. B* **83**, 174432 (2011).
 - ³⁶ S. Miyahara and N. Furukawa, *Phys. Rev. B* **93**, 014445 (2016).
 - ³⁷ M. Matsumoto, K. Chimata, and M. Koga, *J. Phys. Soc. Jpn.* **86**, 034704 (2017).
 - ³⁸ J. Kanamori, *Progr. Theor. Phys.* **30**, 275 (1963).
 - ³⁹ A. Georges, L. de' Medici, and J. Mravlje, *Annu. Rev. Condens. Matter Phys.* **4**, 137 (2013).
 - ⁴⁰ J. C. Slater and G. F. Koster, *Phys. Rev.* **94**, 1498 (1954).
 - ⁴¹ G. Jackeli and G. Khaliullin, *Phys. Rev. Lett.* **102**, 017205 (2009).
 - ⁴² J. G. Rau, E. K.-H. Lee, and H.-Y. Kee, *Phys. Rev. Lett.* **112**, 077204 (2014).
 - ⁴³ Y. Sizyuk, C. Price, P. Wölfle, and N. B. Perkins, *Phys. Rev. B* **90**, 155126 (2014).
 - ⁴⁴ J. G. Rau and H.-Y. Kee, *arXiv:1408.4811* (2014).
 - ⁴⁵ S. M. Winter, Y. Li, H. O. Jeschke, and R. Valentí, *Phys. Rev. B* **93**, 214431 (2016).
 - ⁴⁶ H.-S. Kim and H.-Y. Kee, *Phys. Rev. B* **93**, 155143 (2016).
 - ⁴⁷ R. Yadav, N. A. Bogdanov, V. M. Katukuri, S. Nishimoto, J. van den Brink, and L. Hozoi, *Sci. Rep.* **6**, 37925 (2016).
 - ⁴⁸ S. M. Winter, A. A. Tsirlin, M. Daghofer, J. van den Brink, Y. Singh, P. Gegenwart, and R. Valentí, *J. Phys. Condens. Matter* **29**, 493002 (2017).
 - ⁴⁹ Y. S. Hou, H. J. Xiang, and X. G. Gong, *Phys. Rev. B* **96**, 054410 (2017).
 - ⁵⁰ K. Plumb, J. Clancy, L. Sandilands, V. V. Shankar, Y. Hu, K. Burch, H.-Y. Kee, and Y.-J. Kim, *Phys. Rev. B* **90**, 041112 (2014).
 - ⁵¹ A. Banerjee, C. Bridges, J.-Q. Yan, A. Aczel, L. Li, M. Stone, G. Granroth, M. Lumsden, Y. Yiu, J. Knolle, *et al.*, *Nature materials* **15**, 733 (2016).
 - ⁵² Y. Singh and P. Gegenwart, *Phys. Rev. B* **82**, 064412 (2010).
 - ⁵³ Y. Singh, S. Manni, J. Reuther, T. Berlijn, R. Thomale, W. Ku, S. Trebst, and P. Gegenwart, *Phys. Rev. Lett.* **108**, 127203 (2012).
 - ⁵⁴ N. B. Perkins, Y. Sizyuk, and P. Wölfle, *Phys. Rev. B* **89**, 035143 (2014).
 - ⁵⁵ W. Wang, Z.-Y. Dong, S.-L. Yu, and J.-X. Li, *Phys. Rev. B* **96**, 115103 (2017).
 - ⁵⁶ Our results are similar to those of Ref.⁴⁵ except for t_3 , which might be caused by a different microscopic definition of ϕ .
 - ⁵⁷ D. Torchinsky, H. Chu, L. Zhao, N. Perkins, Y. Sizyuk, T. Qi, G. Cao, and D. Hsieh, *Phys. Rev. Lett.* **114**, 096404 (2015).